Nonlinear viscoelastic analysis of statistically homogeneous random composites

M. Šejnoha, R. Valenta and J. Zeman

Czech Technical University in Prague
Faculty of Civil Engineering
Department of Structural Mechanics
Thákurova 7, 166 29 Prague 6, Czech Republic

ABSTRACT

Owing to the high computational cost in the analysis of large composite structures through a multi-scale or hierarchical modeling an efficient treatment of complex material systems at individual scales is of paramount importance. Limiting the attention to the level of constituents the present paper offers a prosperous modeling strategy for the predictions of nonlinear viscoelastic response of fibrous graphite-epoxy composite systems with possibly random distribution of fibers within a transverse plane section of the composite aggregate. If such a material can be marked as statistically homogeneous and the mechanisms driving the material response fall within the category of first-order homogenization scheme the variational principles of Hashin and Shtrikman emerge as an appealing option in the solution of uncoupled micro-macro computational homogenization. The material statistics up to two-point probability function that are used to describe the morphology of such a microstructure can be then directly incorporated into variational formulations to provide bounds on the effective material response of the assumed composite medium. In the present formulation the Hashin-Shtrikman variational principles are further extended to account for the presence of various transformation fields defined as local eigenstrain or eigenstress distributions in the phases. The evolution of such eigenfields is examined here within the framework of nonlinear viscoelastic behavior of polymeric matrix conveniently described by the Leonov model. Fully implicit integration scheme is implemented to enhance the stability and efficiency of the underlying numerical analysis. In this regard the Fourier transform is called when solving the resulting integral equations, which permits an arbitrary choice of the reference medium so that often encountered anisotropy of individual phases creates no obstacles in the solution procedure. Attention is also paid to the evaluation of the required material statistics. It is shown that replacing the actual microstructure of real world composites with a corresponding digitized image renders a computationally promising numerical approach for their derivation. Apart from application to nonlinear viscoelastic problem the use of the present modeling strategy is further promoted by a good agreement of estimated effective thermoelastic properties with predictions obtained from periodic unit cell models.

KEY WORDS

Fiber-reinforced composite material, Microstructures, Nonlinear viscoelastic processes, Leonov model, Energy methods, Probability and statistics

1. INTRODUCTION

An increasing interest in fabric reinforced composites made of various patterns of stiff graphite fiber tows embedded in a light polymer brings new challenges to an accurate prediction of the mechanical behavior of such complex material systems. To avoid an abstract discussion on this subject we introduce a multi-layered wound composite tube, Fig. 1 to represent a class of composite structures, for which an accurate prediction of mechanical response inevitably requires analyses on different length scales, e.g., a three-scale modeling.

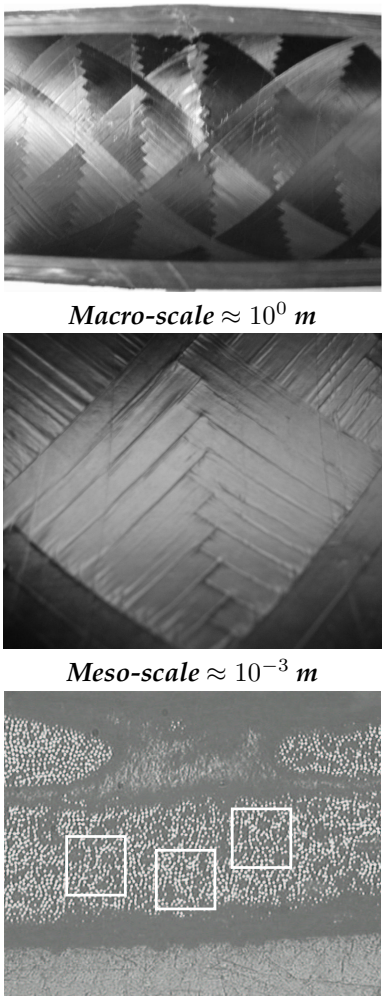

Figure 1: A scheme of three-scale modeling

It is now being widely accepted that novel hierarchical or multi-scale homogenization techniques offer a reliable route in numerical investigation of deformation and failure processes taking place at individual scales [FYS99, KGB02, Mas03].

As generally recognized, a successful completion of this goal calls for an accurate as well as efficient micromechanical modeling starting from the basic building block of a fiber tow impregnated by the matrix phase. As manifested in Fig. 2(a), such a step needs special techniques enabling the determination of effective properties of disordered media. Some promising directions are discussed in papers by [Pov95, ZS01, SZ02b, SG02] and [ZS03]. The essential ingredient of their approach is formulation of a representative volume element in terms of a periodic unit cell consisting of a small number of particles, which statistically resembles the actual composite. Such a unit cell is derived from a simple optimization procedure formulated in terms of various statistical descriptors characterizing the microstructure of the random medium. Once the geometry of the unit cell is specified, well-developed techniques of first-order homogenization (see, e.g., [TD88, MMS99, KBB01]) can be applied to obtain collective properties of analyzed media, ranging from evaluation of the effective thermoelastic properties of random composites to general inelastic analysis of actual material systems under overall thermo-mechanical loading.

Although promising in its potential the procedure may prove to be prohibitively expensive particularly in connection with large multi-scale modeling. If the principle objective becomes reduction of the computational cost particularly on microscale it is provident to appreciate the well known effective medium theories that utilize the Eshelby solution. Being aware of the limits of their validity (e.g., first-order homogenization, applications limited to loading path that induce fiber dominated mode plasticity [DBED87]) one may afford a relatively simple extension of these methods to loading conditions which promote inelastic deformation. A comprehensive overview of applications of these micromechanical techniques combined with the transformation field analysis of Dvorak [Dvo92, DB92] to arrive at the solution of inelastic deformation and other incremental problems in heterogeneous media with many interacting inhomogeneities can be found, e.g., in [DYW94, CKMP01]. Successful implementation within the framework of the Mori-Tanaka method has also been reported in works by [LGN91], [SM99] and [Mat03].

The present contributions expands this class of theories by incorporating elements of real microstructure into formulation of constitutive equations. Here, the

two-point averaging scheme proposed by [FS00] is revisited in conjunction with the Hashin-Shtrikman variational principles [HS63, Wil77] applied to real world material systems. Both the displacement and traction based formulations are presented in view of random composites and extended to account for the presence of initial stresses or strains. Further comments on this subject can be found in [Wil81, PS03].

To keep up with our previous studies on this subject [ZS01, SZ02a, SZ02b], we refer again to the graphite fiber tow embedded in the polymer matrix, Fig. 2(a), to serve as a representative of the two-phase disordered composite medium. Note that Fig. 2(a) represents just one specific cut taken from the fiber two-dimensional cross-section as displayed in Fig. 1(a). Random character of fibers arrangement, typical for such material systems, is conveniently described by the two-point probability function [TS82]. The most appealing feature of this function is the ease and efficiency of its evaluation particularly when taking advantage of the Fast Fourier transform applied to the binary images, Fig. 2(b), of real microstructures [Zem03]. Although higher-order statistical functions such as the three-point probability function may add further knowledge in characterizing the morphology of random composites (see, e.g., [Mar98, Mil02, Tor02]), their evaluation is generally not straightforward and rather expensive especially for high-resolution images of real microstructures and typically relies on the assumption of statistical isotropy.

The overall non-linear response of the present material system is a direct consequence of the behavior of the epoxy matrix that shows significant stress and strain rate sensitivity [KL97]. It has been reported in several papers ([BS02, HAM04] to cite a few) that such a complex non-linear mechanical behavior can be well described either by the Shapery [Sch69] or the generalized Leonov non-linear viscoelastic model [Ter96]. The numerical implementation is usually utilized by converting the general integral equations into a rate-type form employing standard chain models due to Kelvin and Maxwell. Although both chain models provide identical response to a given set of loading and boundary conditions, the Kelvin or Kelvin-Voight is more suitable for creep type of loading thus directly applicable with the dual Hashin-Shtrikman variational principle unlike the Maxwell chain model that admits straightforward solution of the relaxation problem easily utilized with the primary principle. Since the strain control boundary conditions fit well also with the finite element implementation the latter model enhanced by the Leonov type of time-stress superposition and presented within the framework of the primary Hashin-Shtrikman variational principle is examined. Fully implicit integration scheme is used to arrive at a correct convergent state for a given time increment.

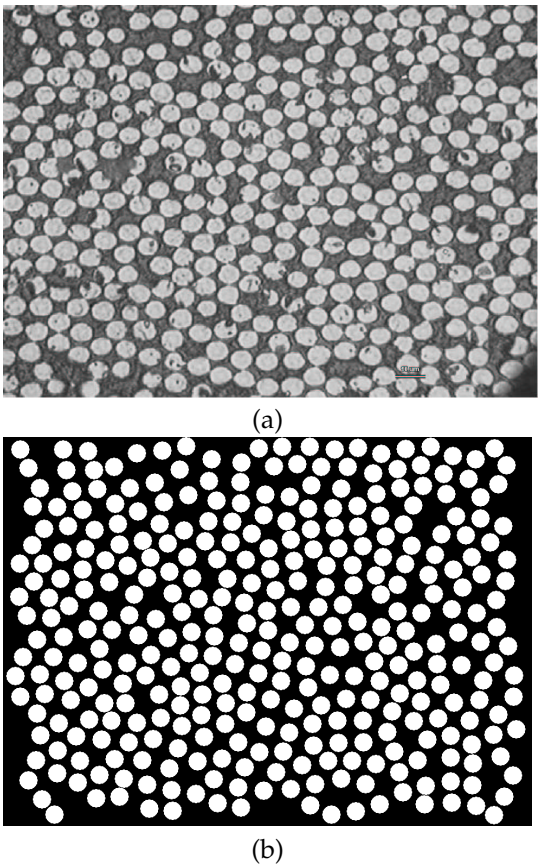

(a)

(b)

Figure 2: (a) A real micrograph (b) a binary image of a transverse plane section of the fiber tow, resolution is 976×716 pixels

In a summary, if we seek for an efficient solution of the nonlinear homogenization problem at least at the lowest scale (with restriction to continuum mechanics) the Hashin-Shtrikman variational principles that allow incorporation of the knowledge of the real microstructure through the two-point probability function appear as a choice worthwhile to explore.

The paper is organized as follows. Section 2 reviews general formulation of the Hashin-Shtrikman variational principles extended for the presence of local eigenstrains or eigenstresses. It further outlines fast numerical procedure based on the Discrete Fourier

Transform for the evaluation of two-point probability function. The procedure draws upon the knowledge of digitized images of real microstructures and the possibility of periodic extension of a representative volume element (RVE). The section closes by comparing the effective thermoelastic properties derived from the present approach with those found from the unit cell analysis [ZS01]. Section 3 presents an implicit formulation of the nonlinear viscoelastic problem that arises from the application of generalized Leonov model. This is followed by several numerical examples that highlight the model applicability. Useful remarks on evaluation of certain microstructure-dependent matrices are given in Appendix A. Appendix B finally comments on several aspects of numerical integration. To keep the discussion simple the analysis is performed in the one-dimensional setting. More information on the material response of the assumed epoxy matrix including experimental results can be found in the upcoming paper [VS03].

In the following text, $\mathbf{a}$, $\boldsymbol{a}$ and $\mathbf{A}$ denote a vector, a symmetric second-order and a fourth-order tensor, respectively. The standard summation notation is adopted, i.e., by $\mathbf{A} : \boldsymbol{b}$ denotes the sum $A_{ijkl}b_{kl}$ while $\mathbf{a} \cdot \mathbf{b}$ stands for $a_i b_i$, where the summation with respect to repeated indices is used. The symbol $\{\mathsf{a}\}$ is reserved for a column matrix or a vectorial representation of symmetric second-order tensor while the notation $[\mathsf{L}]$ is employed for a matrix representation of a fourth-order tensor [BS96]. $\widetilde{f}$ will be used to denote the Fourier transform of a given function f. Finally, note that the state of generalized plane strain [MMS99, Appendix B] with x_3 being the axis of fibers is assumed in the whole analysis.

2. MACROSCOPIC CONSTITUTIVE EQUATIONS

To introduce the subject, consider a material element having a length scale sufficiently large compared to the microstructural one so it can be treated as statistically representative of the composite. With reference to the scope of the current work, we further limit our knowledge of microstructural configuration to the description by two-point probability functions, see Section 2.1. Such a limited characterization still contains substantially more information compared to the description by volume fractions only and it is quite beneficial to the numerical analysis as it allows relatively simple application of the Hashin-Shtrikman variational principles for incorporating microstructural information beyond that contained in the volume fractions.

In particular, Hashin and Shtrikman [HS62] presented two alternative representations of energy functions by introducing polarization fields relative to a homogeneous reference (comparison) medium. In Sections 2.2 and 2.3, we focus on theoretical aspects associated with the variational formulation for anisotropic and non-homogeneous bodies with either prescribed displacements $\mathbf{u} = \overline{\mathbf{u}}$ or tractions $\mathbf{p} = \overline{\mathbf{p}}$ along the entire boundary S of the composite. In addition, eigenstrains (stress free strains) or eigenstresses are admitted in the present formulation. Successful predictions of thermoelastic effective properties derived for the material system of Fig. 2(a) are presented in Section 2.4 to motivate the subsequent analysis of materials showing nonlinear and time-dependent behavior.

2.1. Evaluation of two-point probability functions

To begin, consider a sample space $\mathcal{S}$ defined here as a collection of material elements similar to one of Fig. 2(a). Random nature of the present material system further suggests that individual members of $\mathcal{S}$, to be statistically representative of the composite, should be sufficiently large compared to the microstructural length scale (e.g., fiber diameter). Apart from such a classical representation of a material representative volume element (RVE) we pose an additional, perhaps more concrete, requirement on the minimum size of the RVE. In particular, from the prospective of micromechanical analysis to come we shall require the size of the RVE to be *at least* such that one can identify two points, both contained by the RVE, which are statistically independent.

Such a sample space $\mathcal{S}$ is called an *ensemble* – the collection of a large number of systems that are different in their microscopical details but identical in their macroscopic details. Formation of $\mathcal{S}$ then opens a way to provide an estimate for effective or expected value of some quantity, say stress or strain field, through the process of its averaging over all systems in the ensemble. To proceed, label individual members of this space by α and define $p(\alpha)$ as the probability density of α in $\mathcal{S}$ (see, e.g., [DW96, Wil77]) for further reference). Then, the *ensemble average* of function $F(\mathbf{x}, \alpha)$ at a point $\mathbf{x}$ is provided by

$$\overline{F(\mathbf{x})} = \int_{\mathcal{S}} F(\mathbf{x}, \alpha) p(\alpha) \mathrm{d}\alpha. \tag{2.1}$$

Hereafter, we limit our attention to a two-phase random medium. To provide a general statistical description of such a system it proves useful to characterize each member of the ensemble by a stochastic function – *characteristic* function $\chi_r(\mathbf{x},\alpha)$, which equals to one when a point $\mathbf{x}$ lies in a phase r in the sample α and equals to zero otherwise [Ber68, TS82],

$$\chi_r(\mathbf{x},\alpha) = \begin{cases} 1 & \mathbf{x} \in D_r(\alpha) \\ 0 & \text{otherwise} \end{cases}, \tag{2.2}$$

where $D_r(\alpha)$ denotes the domain occupied by the r-th phase; r is further assumed to take values m for the matrix phase while symbol f is reserved for the second phase. Except where noted, a fibrous composite with aligned impenetrable fibers having circular cross-section of equal radius is considered. For such a system the characteristic functions $\chi_f(\mathbf{x},\alpha)$ and $\chi_m(\mathbf{x},\alpha)$ are related by

$$\chi_m(\mathbf{x},\alpha) + \chi_f(\mathbf{x},\alpha) = 1. \tag{2.3}$$

With regard to the potential application of H-S variational principles it is sufficient to quantify the morphology of random medium by the *one-point probability* function $S_r(\mathbf{x})$

$$S_r(\mathbf{x}) = \overline{\chi_r(\mathbf{x},\alpha)}, \tag{2.4}$$

which simply gives the probability of finding the phase r at $\mathbf{x}$ and by the *two-point probability* function $S_{rs}(\mathbf{x},\mathbf{x}')$

$$S_{rs}(\mathbf{x},\mathbf{x}') = \overline{\chi_r(\mathbf{x},\alpha)\chi_s(\mathbf{x}',\alpha)}, \tag{2.5}$$

which denotes the probability of finding simultaneously phase r at $\mathbf{x}$ and phase s at $\mathbf{x}'$. When regarding the material as ergodic and statistically homogeneous Eqs. (2.4) and (2.5) become

$$S_r(\mathbf{x}) = c_r, \tag{2.6}$$

$$S_{rs}(\mathbf{x},\mathbf{x}') = S_{rs}(\mathbf{x}-\mathbf{x}'), \tag{2.7}$$

where c_r is the volume fraction of the r-th phase (see [ZS01] for testing statistical hypotheses).

In evaluation of the two-point probability function S_{rs} we introduce a binary version of Fig. 2(a). Such a digitized micrograph, Fig. 2(b), can be imagined as a discretization of the characteristic function $\chi_r(\mathbf{x},\alpha)$, presented in terms of a $M \times N$ bitmap. Denoting the value of χ_r for the pixel located in the i^{th} row and j^{th} column as a $\chi_r(i,j)$ allows writing the function S_m for an ergodic and statistically homogeneous medium in the form

$$S_r = \frac{1}{MN}\sum_{i=1}^{M}\sum_{j=1}^{N}\chi_r(i,j) \tag{2.8}$$

while, under assumption of periodicity of analyzed media, the two-point probability function S_{rs} assumes the form

$$S_{rs}(m,n) = \frac{1}{MN}\sum_{i=1}^{M}\sum_{j=1}^{N}\chi_r(i,j)\chi_s((i+m)\%M,(j+n)\%N), \tag{2.9}$$

where symbol "%" stands for modulo. The number of operations needed to evaluate the sum (2.9) can be substantially reduced when using the fast Fourier transform algorithm [Ber84]. Indeed, recognizing that (2.9) is the cyclic correlation [BP85], the Discrete Fourier Transform (DFT) of this function is given by the following relation

$$\mathrm{DFT}\{S_{rs}(m,n)\} = \mathrm{DFT}\{\chi_r(m,n)\}\overline{\mathrm{DFT}\{\chi_s(m,n)\}}, \tag{2.10}$$

where $\bar{\cdot}$ now stands for a complex conjugate. The inverse DFT denoted as IDFT then serves to derive function S_{rs} at the final set of discrete points as

$$S_{rs}(m,n) = \mathrm{IDFT}\{\mathrm{DFT}\{\chi_r(m,n)\}\overline{\mathrm{DFT}\{\chi_s(m,n)\}}\}. \tag{2.11}$$

Usually, the Fast Fourier Transform [EJ98], which needs only $MN(\log(MN))$ operations, is called to carry out the numerical computation.

Fig. 3(a) shows the two–point matrix probability function S_{mm} obtained for the 488×358 resolution of the digitized medium. In addition, the isotropized values of the two-point probability function, derived for different resolution of digitized media, are shown in Fig. 3(b). Evidently, even rather coarse resolution of analyzed bitmap is sufficient to obtain these functions with a high degree of precision, which can substantially reduce the computational time needed for evaluation of this function, see Table 1.

Bitmap resolution		
976×716	488×358	244×179
6.24	1.54	0.37

Table 1: CPU time in seconds required to evaluate function S_{mm}

The final comment reconciles the true behavior of function S_{rs} and its periodic character which results from Eq. (2.11). Recall that for large values of $\|\mathbf{x}\|$, we require two points to be statistically independent, i.e. $S_{mm}(\mathbf{x}) \longrightarrow c_m^2$. Therefore, the sample size should be sufficiently large to comply with this

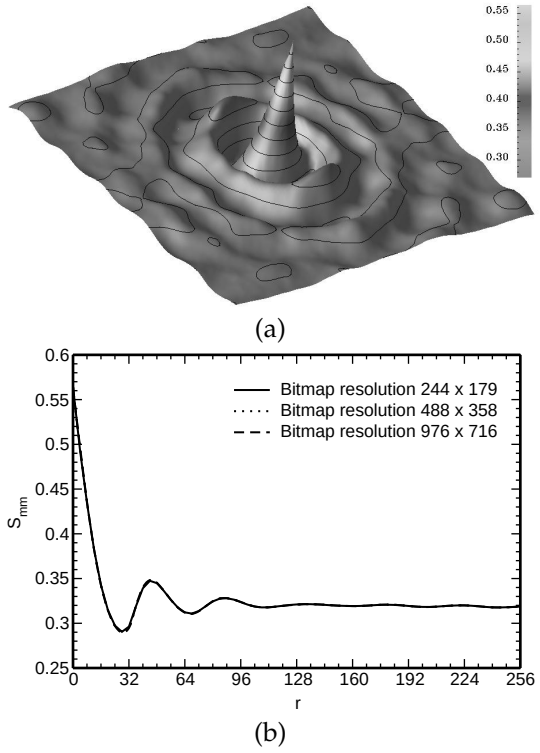

Figure 3: Two-point matrix matrix probability S_{mm} function derived for a digitized medium, (a) Example of the function, (b) Effect of bitmap resolution

property. As illustrated in Fig. 3(b) this requirement is certainly fulfilled for the present sample. Recall one specific example shown in Figs. 2(b) taken as a random cut from various locations in the fiber tow as displayed in Fig. 1(c).

2.2. Strain control approach

With reference to the general problem displayed in Fig. 4 we consider an anisotropic and heterogeneous body loaded by an affine displacement field $\boldsymbol{u}_0(\mathbf{x}) = \boldsymbol{E} \cdot \mathbf{x}$. The local constitutive law including eigenstresses $\boldsymbol{\lambda}$ then reads

$$\begin{aligned} \boldsymbol{\sigma}(\mathbf{x}) = \mathbf{L}(\mathbf{x}) : \boldsymbol{\varepsilon}(\mathbf{x}) + \boldsymbol{\lambda}(\mathbf{x}) \qquad & \text{in } \Omega, \\ \mathbf{u} = \overline{\mathbf{u}} \qquad & \text{on } S. \end{aligned} \tag{2.12}$$

As suggested by Hashin-Shtrikman [HS62] the local stress and strain fields in Eq. (2.12) can be found from the two auxiliary boundary value problems, Fig. 4. The procedure starts by assuming a geometrically identical body with a certain reference homogeneous, but generally anisotropic, medium $\mathbf{L}_0$ and the same prescribed displacements. The corresponding uniform strain $\boldsymbol{E}$ and stress $\boldsymbol{\Sigma}$ fields are related through constitutive law in the form

$$\boldsymbol{\Sigma} = \mathbf{L}_0 : \boldsymbol{E} \quad \text{in } \Omega, \quad \mathbf{u}_0 = \overline{\mathbf{u}} \text{ on } S. \tag{2.13}$$

Following the Hashin-Shtrikman idea, we introduce the symmetric stress polarization tensor $\boldsymbol{\tau}$ such that

$$\boldsymbol{\sigma}(\mathbf{x}) = \mathbf{L}_0 : \boldsymbol{\varepsilon}(\mathbf{x}) + \boldsymbol{\tau}(\mathbf{x}). \tag{2.14}$$

In addition, denote

$$\begin{aligned} \mathbf{u}' = \mathbf{u} - \mathbf{u}_0(\mathbf{x}) \qquad & \text{in } \Omega, \\ \mathbf{u}' = \mathbf{0} \qquad & \text{on } S, \end{aligned} \tag{2.15}$$

and

$$\boldsymbol{\varepsilon}'(\mathbf{x}) = \boldsymbol{\varepsilon} - \boldsymbol{E} \qquad \text{in } \Omega, \tag{2.16}$$

$$\boldsymbol{\sigma}'(\mathbf{x}) = \boldsymbol{\sigma} - \boldsymbol{\Sigma} \qquad \text{in } \Omega. \tag{2.17}$$

The objective is to formulate a variational principle describing the behavior of the nonhomogeneous anisotropic material subjected to known eigenstresses and prescribed boundary displacements. Schematic representation of this problem is displayed in Fig. 4. Provided that both $\boldsymbol{\sigma}$ and $\boldsymbol{\Sigma}$ fields are statically admissible, the following equations have to be satisfied (see, e.g., [BS96]),

$$\boldsymbol{\nabla} \cdot (\mathbf{L}_0 : \boldsymbol{\varepsilon} + \boldsymbol{\tau}) = \mathbf{0} \quad \text{in } \Omega, \tag{2.18}$$

$$\boldsymbol{\tau} - (\mathbf{L} - \mathbf{L}_0) : \boldsymbol{\varepsilon} - \boldsymbol{\lambda} = \mathbf{0} \quad \text{in } \Omega, \tag{2.19}$$

$$\mathbf{u}' = \mathbf{0} \quad \text{on } S. \tag{2.20}$$

A formulation equivalent to Eqs. (2.18) and (2.19) may be obtained by performing a variation of the extended functional

$$\begin{aligned} U_{\boldsymbol{\tau}} = \frac{1}{2} \int_\Omega \big(\boldsymbol{E} : \boldsymbol{\Sigma} - (\boldsymbol{\tau} - \boldsymbol{\lambda}) : (\mathbf{L} - \mathbf{L}_0)^{-1} : (\boldsymbol{\tau} - \boldsymbol{\lambda}) + \\ + 2\boldsymbol{\tau} : \boldsymbol{E} + \boldsymbol{\varepsilon}' : \boldsymbol{\tau} + \boldsymbol{\lambda} : \mathbf{L}^{-1} : \boldsymbol{\lambda} \big) \, \mathrm{d}\Omega. \end{aligned} \tag{2.21}$$

Setting

$$\begin{aligned} \delta U_{\boldsymbol{\tau}} = & -\frac{1}{2} \int_\Omega \{ 2\delta\boldsymbol{\tau} : [(\mathbf{L} - \mathbf{L}_0)^{-1} : (\boldsymbol{\tau} - \boldsymbol{\lambda}) - \boldsymbol{\varepsilon}] + \\ & + \delta\boldsymbol{\tau} : \boldsymbol{\varepsilon}' - \delta\boldsymbol{\varepsilon}' : \boldsymbol{\tau} \} \mathrm{d}\Omega = 0, \end{aligned} \tag{2.22}$$

we find that Eq. (2.19) is one of the stationarity conditions of $U_{\boldsymbol{\tau}}$, while the second condition, Eq. (2.18), follows after recasting the remaining terms in the brackets. Finally, it can be proven that the stationary value $U_{\boldsymbol{\tau}}^S$ of the potential $U_{\boldsymbol{\tau}}$ equals the actual

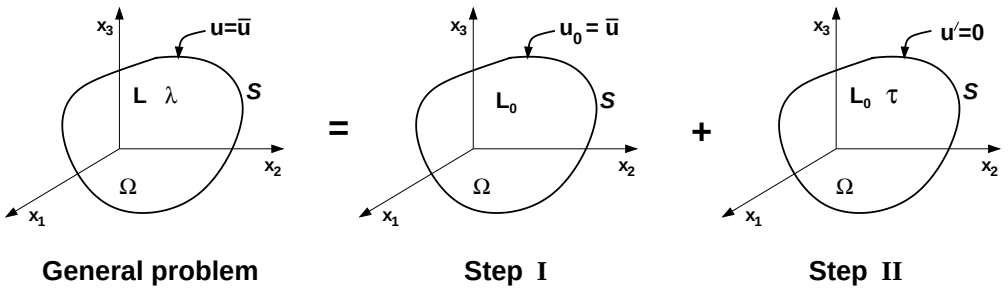

Figure 4: Body with prescribed surface displacements including eigenstresses

potential energy stored in the anisotropic heterogeneous body

$$U^S_{\boldsymbol{\tau}} = \frac{1}{2}\int_\Omega (\boldsymbol{\varepsilon}-\boldsymbol{\mu}) : \mathbf{L} : (\boldsymbol{\varepsilon}-\boldsymbol{\mu}) \mathrm{d}\Omega, \tag{2.23}$$

where $\boldsymbol{\mu} = -\mathbf{L}^{-1}\boldsymbol{\lambda}$ is the vector of eigenstrains (stress-free strains). The functional $U_{\boldsymbol{\tau}}$ attains its maximum ($\delta^2 U_{\boldsymbol{\tau}} < 0$) if $(\mathbf{L}-\mathbf{L}_0)$ is positive definite and its minimum if $(\mathbf{L}-\mathbf{L}_0)$ is negative definite.
To make use of H-S functional, Eq. (2.21), or its variation, Eq. (2.22), one has to express $\boldsymbol{\varepsilon}'$ via the polarization tensor $\boldsymbol{\tau}$

$$\begin{aligned} \boldsymbol{\varepsilon}'(\mathbf{x}) &= \boldsymbol{\varepsilon}(\mathbf{x}) - \boldsymbol{E} \\ &= \int_\Omega \epsilon^*_{\mathbf{0}}(\mathbf{x}-\mathbf{x}') : (\boldsymbol{\tau}(\mathbf{x}') - \langle\boldsymbol{\tau}\rangle)\, \mathrm{d}\mathbf{x}' \\ &= \left[\epsilon^*_{\mathbf{0}}\,(\boldsymbol{\tau} - \langle\boldsymbol{\tau}\rangle)\right], \end{aligned} \tag{2.24}$$

where $\langle\cdot\rangle$ represents a volume average of a given quantity. Detailed derivation of the operator $[\epsilon^*_{\mathbf{0}}\,(\boldsymbol{\tau} - \langle\boldsymbol{\tau}\rangle)]$ can be found, e.g, in [Krö86, Mur87, Wil77] and Appendix A. Subscript 0 is used to identify this operator with the homogeneous reference medium. Introducing Eq. (2.24) into Eq. (2.21) gives

$$\begin{aligned} U_{\boldsymbol{\tau}} = \frac{1}{2}\int_\Omega \Big(& \boldsymbol{E} : \boldsymbol{\Sigma} - (\boldsymbol{\tau}(\mathbf{x}) - \boldsymbol{\lambda}(\mathbf{x})) : (\mathbf{L}(\mathbf{x}) - \mathbf{L}_0)^{-1} : \\ & : (\boldsymbol{\tau}(\mathbf{x}) - \boldsymbol{\lambda}(\mathbf{x})) + 2\boldsymbol{\tau}(\mathbf{x}) : \boldsymbol{E} + \boldsymbol{\tau}(\mathbf{x}) : \\ & : \int_\Omega \epsilon^*_{\mathbf{0}}(\mathbf{x}-\mathbf{x}') : (\boldsymbol{\tau}(\mathbf{x}') - \langle\boldsymbol{\tau}\rangle)\, \mathrm{d}\mathbf{x}' + \\ & + \boldsymbol{\lambda}(\mathbf{x}) : \mathbf{L}^{-1}(\mathbf{x}) : \boldsymbol{\lambda}(\mathbf{x}) \Big) \mathrm{d}\mathbf{x}. \end{aligned} \tag{2.25}$$

If each phase r of a randomly arranged composite is homogeneous with moduli $\mathbf{L}_r, r = 1, \ldots, n$, then the material stiffness matrix in the sample α can be expressed as [DW96],

$$\mathbf{L}(\mathbf{x}, \alpha) = \sum_{r=1}^{n} \mathbf{L}_r \chi_r(\mathbf{x}, \alpha). \tag{2.26}$$

With the help of Eq. (2.4), the ensemble average of $\mathbf{L}$ is

$$\overline{\mathbf{L}(\mathbf{x})} = \sum_{r=1}^{n} \mathbf{L}_r S_r(\mathbf{x}). \tag{2.27}$$

Similarly, the trial fields for $\boldsymbol{\tau}$ and eigenstress $\boldsymbol{\lambda}$ at any point $\mathbf{x}$ located in the sample α are provided by

$$\boldsymbol{\tau}(\mathbf{x}, \alpha) = \sum_{r=1}^{n} \boldsymbol{\tau}_r(\mathbf{x}) \chi_r(\mathbf{x}, \alpha), \tag{2.28}$$

$$\boldsymbol{\lambda}(\mathbf{x}, \alpha) = \sum_{r=1}^{n} \boldsymbol{\lambda}_r(\mathbf{x}) \chi_r(\mathbf{x}, \alpha), \tag{2.29}$$

with the respective ensemble averages written as

$$\overline{\boldsymbol{\tau}(\mathbf{x})} = \sum_{r=1}^{n} \boldsymbol{\tau}_r(\mathbf{x}) S_r(\mathbf{x}), \tag{2.30}$$

$$\overline{\boldsymbol{\lambda}(\mathbf{x})} = \sum_{r=1}^{n} \boldsymbol{\lambda}_r(\mathbf{x}) S_r(\mathbf{x}). \tag{2.31}$$

To facilitate the solution of the present problem the material is assumed to be ergodic and statistically homogeneous. Therefore,

$$\overline{\mathbf{L}} = \sum_{r=1}^{n} \mathbf{L}_r c_r, \qquad \overline{\boldsymbol{\tau}(\mathbf{x})} = \sum_{r=1}^{n} \boldsymbol{\tau}_r(\mathbf{x}) c_r, \qquad \overline{\boldsymbol{\lambda}(\mathbf{x})} = \sum_{r=1}^{n} \boldsymbol{\lambda}_r(\mathbf{x}) c_r. \tag{2.32}$$

Substituting Eqs. (2.28) and (2.32) into Eq. (2.25) yields the averaged form of the extended Hashin-

Shtrikman principle

$$\begin{aligned}\overline{U}_{\boldsymbol{\tau}} = \frac{1}{2}\int_\Omega \Big(\boldsymbol{E}:\boldsymbol{\Sigma} + \sum_r c_r \boldsymbol{\lambda}_r(\mathbf{x}):\mathbf{L}_r:\boldsymbol{\lambda}_r(\mathbf{x})\Big)\mathrm{d}\mathbf{x} - \\ - \frac{1}{2}\sum_{r=1}^n \int_\Omega \Big(c_r(\boldsymbol{\tau}_r(\mathbf{x}) - \boldsymbol{\lambda}_r(\mathbf{x})):(\mathbf{L}_r - \mathbf{L}_0)^{-1}: \\ :(\boldsymbol{\tau}_r(\mathbf{x}) - \boldsymbol{\lambda}_r(\mathbf{x})) - 2c_r\boldsymbol{\tau}_r:(\mathbf{x})\boldsymbol{E}\Big)\mathrm{d}\mathbf{x} + \\ + \frac{1}{2}\sum_{r=1}^n\sum_{s=1}^n \int_\Omega \boldsymbol{\tau}_r(\mathbf{x}):\int_\Omega \epsilon_{\mathbf{0}}^*(\mathbf{x}-\mathbf{x}'): \\ :[S_{rs}(\mathbf{x}-\mathbf{x}')\boldsymbol{\tau}_s(\mathbf{x}') - c_r\langle\boldsymbol{\tau}\rangle]\,\mathrm{d}\mathbf{x}'\mathrm{d}\mathbf{x}.\end{aligned}$$

Assuming a piecewise uniform variation of eigenstress vector $\boldsymbol{\lambda}$ and polarization stress $\boldsymbol{\tau}$ ($\boldsymbol{\lambda}_r(\mathbf{x}) = \boldsymbol{\lambda}_r, \boldsymbol{\tau}_r(\mathbf{x}) = \boldsymbol{\tau}_r$), setting $\langle\boldsymbol{\tau}\rangle = \sum_r \boldsymbol{\tau}_r c_r$ and then performing variation with respect to $\boldsymbol{\tau}_r$ provides the extended form of the stationarity conditions. Employing the engineering notation, the stationary conditions yield the following system of linear equations

$$\begin{aligned}\sum_{s=1}^n \left(\delta_{rs}([\mathsf{L_r}] - [\mathsf{L_0}])^{-1}c_r - [\mathsf{A_{rs}}]\right)\{\tau_s\} = \\ \{\mathsf{E}\}c_r + ([\mathsf{L_r}] - [\mathsf{L_0}])^{-1}\{\lambda_r\}c_r,\end{aligned} \tag{2.33}$$

where $r = 1, \ldots, n$. The microstructure-dependent matrices $[\mathsf{A_{rs}}]$ are independent of $\mathbf{x}$ and are provided by

$$[\mathsf{A_{rs}}] = \int_\Omega [\epsilon_0^*]\,(\mathbf{x}-\mathbf{x}')\,(S_{rs}(\mathbf{x}-\mathbf{x}') - c_r c_s)\,\mathrm{d}\mathbf{x}'. \tag{2.34}$$

A symbolic inversion of the system (2.33) gives the solution for unknown components of the polarization stress $\{\tau_r\}$ in the form[1]

$$\{\tau_r\} = \sum_{s=1}^n c_s\,[\mathsf{T_{rs}}]\left(\{\mathsf{E}\} + ([\mathsf{L_s}] - [\mathsf{L_0}])^{-1}\{\lambda_s\}\right), \tag{2.35}$$

from which

$$\{\overline{\tau}\} = \sum_{r=1}^n\sum_{s=1}^n c_r c_s\,[\mathsf{T_{rs}}]\left(\{\mathsf{E}\} + ([\mathsf{L_s}] - [\mathsf{L_0}])^{-1}\{\lambda_s\}\right). \tag{2.36}$$

Hence, according to (2.12) and (2.14), the overall constitutive law can be written as

$$\{\Sigma\} = \left[\mathsf{L}^{\mathsf{HS}}\right]\{\mathsf{E}\} + \{\Lambda^{\mathsf{HS}}\}, \tag{2.37}$$

[1]Note that matrices $[\mathsf{T_{rs}}]$ correspond to individual blocks of the inverse to the left-hand side matrix of the system (2.33).

where

$$\begin{aligned}\left[\mathsf{L}^{\mathsf{HS}}\right] &= [\mathsf{L_0}] + \sum_{r=1}^n\sum_{s=1}^n c_r c_s\,[\mathsf{T_{rs}}], \\ \{\Lambda^{\mathsf{HS}}\} &= \sum_{r=1}^n\sum_{s=1}^n c_r c_s\,[\mathsf{T_{rs}}]\,([\mathsf{L_s}] - [\mathsf{L_0}])^{-1}\{\lambda_s\}.\end{aligned} \tag{2.38}$$

In general, solving Eq. (2.33) calls for an efficient method to tackle Eq. (2.34). A suitable method of attack for obtaining the matrices $[\mathsf{A_{rs}}]$ numerically for a binary representation of real microstructures is presented in Appendix A. In addition, explicit forms of matrices $[\mathsf{T_{rs}}]$ for a two-phase medium are provided.

2.3. Stress control approach

Recall that the primary variational principle of Hashin and Shtrikman Eq. (2.21), modified to account for the presence of initial stresses, can be used to derive the effective stiffness matrix $\left[\mathsf{L}^{\mathsf{HS}}\right]$ and overall eigenstress $\{\Lambda^{\mathsf{HS}}\}$ of the composite medium. Similarly, employing its dual counterpart one may arrive at the effective compliance matrix $\left[\mathsf{M}^{\mathsf{HS}}\right]$ and overall eigenstrain $\{\Upsilon^{\mathsf{HS}}\}$. In such a case the boundary value problem discussed in Section 2.2 is modified according to Fig. 5.

In particular, suppose that surface tractions $\overline{\boldsymbol{p}} = \boldsymbol{\Sigma}\cdot\mathbf{n}$ compatible with a uniform stress $\boldsymbol{\Sigma}$ are applied along the boundary S of a homogeneous comparison medium (Step I) characterized by the compliance matrix $\mathbf{M}_0$. The corresponding uniform strain $\boldsymbol{E}$ then follows from the constitutive law

$$\boldsymbol{E} = \mathbf{M}_0:\boldsymbol{\Sigma} \qquad \text{in } \Omega, \tag{2.39}$$

$$\mathbf{p}_0 = \overline{\mathbf{p}} \qquad \text{on } S. \tag{2.40}$$

The local stress $\boldsymbol{\sigma}(\mathbf{x})$ at a point $\mathbf{x}$ in Ω of a composite is found by superimposing the solution of the local problem displayed in Fig. 5 Step II. The respective governing equations then read

$$\boldsymbol{\varepsilon}(\mathbf{x}) = \mathbf{M}(\mathbf{x}):\boldsymbol{\sigma}(\mathbf{x}) + \boldsymbol{\mu}(\mathbf{x}) \qquad \text{on } \Omega, \tag{2.41}$$

$$\mathbf{p} = \overline{\mathbf{p}} \qquad \text{on } S. \tag{2.42}$$

$$\boldsymbol{\varepsilon}(\mathbf{x}) = \mathbf{M}_0:\boldsymbol{\sigma}(\mathbf{x}) + \boldsymbol{\gamma}(\mathbf{x}) \qquad \text{in } \Omega, \tag{2.43}$$

$$\begin{aligned}0 = {}&\varepsilon'_{ij,kl}(\mathbf{x}) + \varepsilon'_{kl,ij}(\mathbf{x}) \\ &- \varepsilon'_{ik,jl}(\mathbf{x}) - \varepsilon'_{jl,ik}(\mathbf{x}) \qquad \text{in } \Omega,\end{aligned} \tag{2.44}$$

$$\boldsymbol{\gamma}(\mathbf{x}) = (\mathbf{M}(\mathbf{x}) - \mathbf{M}_0):\boldsymbol{\sigma}(\mathbf{x}) + \boldsymbol{\mu}(\mathbf{x}) \qquad \text{in } \Omega, \tag{2.45}$$

$$\mathbf{p}'(\mathbf{x}) = \mathbf{p}(\mathbf{x}) - \mathbf{p}_0 \qquad \text{in } \Omega, \tag{2.46}$$

$$\mathbf{p}' = \mathbf{0} \qquad \text{on } S, \tag{2.47}$$

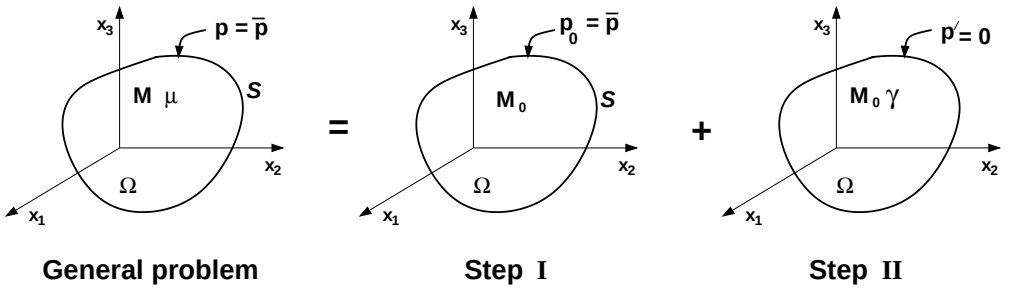

Figure 5: Body with prescribed surface tractions including eigenstrains

where $\boldsymbol{\mu}(\mathbf{x})$ is the local eigenstrain and $\boldsymbol{\gamma}(\mathbf{x})$ is called the polarization strain. The compatibility equation (2.44) together with Eq. (2.45) follow from the extended energy functional given by

$$U_{\boldsymbol{\gamma}} = \frac{1}{2}\int_{\Omega}\Big(\boldsymbol{\Sigma}:\boldsymbol{E}-(\boldsymbol{\gamma}-\boldsymbol{\mu}):(\mathbf{M}-\mathbf{M}_0)^{-1}:(\boldsymbol{\gamma}-\boldsymbol{\mu})+ \\ +2\boldsymbol{\gamma}:\boldsymbol{\Sigma}+\boldsymbol{\sigma}':\boldsymbol{\gamma}\Big)\mathrm{d}\Omega. \quad (2.48)$$

Again, performing a variation with respect to unknown quantities $\boldsymbol{\gamma}$ and $\boldsymbol{\sigma}'$ yields

$$\delta U_{\boldsymbol{\gamma}} = -\frac{1}{2}\int_{\Omega}\{2\delta\boldsymbol{\gamma}:[(\mathbf{M}-\mathbf{M}_0)^{-1}:(\boldsymbol{\gamma}-\boldsymbol{\mu})-\boldsymbol{\sigma}]+ \\ + \delta\boldsymbol{\gamma}:\boldsymbol{\sigma}'-\delta\boldsymbol{\sigma}':\boldsymbol{\gamma}\}\mathrm{d}\Omega. \quad (2.49)$$

Setting $\delta U_{\boldsymbol{\gamma}} = 0$ we immediately recover Eq. (2.45), while the compatibility condition, Eq. (2.44), follows after recasting the remaining terms in the brackets. As for the primary variational principle, it can be proven that the stationary value $U^S_{\boldsymbol{\gamma}}$ of the potential $U_{\boldsymbol{\gamma}}$ equals the actual complementary energy stored in the anisotropic and heterogeneous body

$$U^S_{\boldsymbol{\gamma}} = \frac{1}{2}\int_{\Omega}(\boldsymbol{\sigma}:\mathbf{M}:\boldsymbol{\sigma}+2\boldsymbol{\sigma}:\boldsymbol{\mu})\mathrm{d}\Omega. \quad (2.50)$$

The functional $U_{\boldsymbol{\gamma}}$ attains its maximum ($\delta^2 U_{\boldsymbol{\gamma}} < 0$) if $(\mathbf{M}-\mathbf{M}_0)$ is positive definite and its minimum if $(\mathbf{M}-\mathbf{M}_0)$ is negative definite.

To reduce the number of unknown quantities we first write $\boldsymbol{\sigma}'$ in terms of the polarization strain $\boldsymbol{\gamma}$ in the form

$$\boldsymbol{\sigma}'(\mathbf{x}) = \boldsymbol{\sigma}(\mathbf{x})-\boldsymbol{\Sigma} = \int_{\Omega}\sigma^*_{\mathbf{0}}(\mathbf{x}-\mathbf{x}'):\big(\boldsymbol{\gamma}(\mathbf{x}')-\langle\boldsymbol{\gamma}\rangle\big)\mathrm{d}\mathbf{x}'- \\ -\mathbf{M}_0^{-1}:\big(\boldsymbol{\gamma}(\mathbf{x})-\langle\boldsymbol{\gamma}\rangle\big) = [\sigma^*_{\mathbf{0}}\,(\boldsymbol{\gamma}-\langle\boldsymbol{\gamma}\rangle)] \quad (2.51)$$

The operator $[\sigma^*_{\mathbf{0}}\,(\boldsymbol{\gamma}-\langle\boldsymbol{\gamma}\rangle)]$ can be identified with the operator $[\epsilon^*_{\mathbf{0}}\,(\boldsymbol{\tau}-\langle\boldsymbol{\tau}\rangle)]$ when replacing $\boldsymbol{\gamma}$ for $\boldsymbol{\tau}$ and $\sigma^*_{\mathbf{0}}$ for $\epsilon^*_{\mathbf{0}}$ and suitably modifying the boundary term to reflect the traction boundary conditions [Krö86, Wil77]. Properties of tensor $\epsilon^*_{\mathbf{0}}$ and $\sigma^*_{\mathbf{0}}$ are, for reader's convenience, summarized in Appendix A. Again, subscript 0 refers to the homogeneous reference medium.

Next, in analogy with the primary principle, we introduce Eq. (2.51) into the dual variational principle Eq. (2.48) to get

$$U_{\boldsymbol{\gamma}} = \frac{1}{2}\int_{\Omega}\Big(\boldsymbol{\Sigma}:\boldsymbol{E}-(\boldsymbol{\gamma}(\mathbf{x})-\boldsymbol{\mu}(\mathbf{x})):(\mathbf{M}(\mathbf{x})-\mathbf{M}_0)^{-1}: \\ :(\boldsymbol{\gamma}(\mathbf{x})-\boldsymbol{\mu}(\mathbf{x}))+2\boldsymbol{\gamma}(\mathbf{x}):\boldsymbol{\Sigma}+\boldsymbol{\gamma}(\mathbf{x}):\int_{\Omega}\sigma^*_{\mathbf{0}}(\mathbf{x}-\mathbf{x}'): \\ :\big(\boldsymbol{\gamma}(\mathbf{x}')-\langle\boldsymbol{\gamma}\rangle\big)\,\mathrm{d}\mathbf{x}'-\boldsymbol{\gamma}(\mathbf{x}):\mathbf{M}_0^{-1}:\big(\boldsymbol{\gamma}(\mathbf{x})-\langle\boldsymbol{\gamma}\rangle\big)\Big)\mathrm{d}\mathbf{x} \quad (2.52)$$

Assuming that each phase r of a randomly arranged composite is homogeneous with the compliance matrix $\mathbf{M}_r, r = 1,\ldots,n$, we write in analogy with Section 2.2 the material compliance matrix, the polarization strain $\boldsymbol{\gamma}$ and eigenstrain $\boldsymbol{\mu}$ in the sample α as

$$\mathbf{M}(\mathbf{x},\alpha) = \sum_{r=1}^{n}\mathbf{M}_r\chi_r(\mathbf{x},\alpha), \quad (2.53)$$
$$\boldsymbol{\gamma}(\mathbf{x},\alpha) = \sum_{r=1}^{n}\boldsymbol{\gamma}_r(\mathbf{x})\chi_r(\mathbf{x},\alpha),$$
$$\boldsymbol{\mu}(\mathbf{x},\alpha) = \sum_{r=1}^{n}\boldsymbol{\mu}_r(\mathbf{x})\chi_r(\mathbf{x},\alpha),$$

with the respective ensemble averages given by

$$\overline{\mathbf{M}(\mathbf{x})} = \sum_{r=1}^{n}\mathbf{M}_r S_r(\mathbf{x}), \qquad \overline{\boldsymbol{\gamma}(\mathbf{x})} = \sum_{r=1}^{n}\boldsymbol{\gamma}_r(\mathbf{x})S_r(\mathbf{x}),$$
$$\overline{\boldsymbol{\mu}(\mathbf{x})} = \sum_{r=1}^{n}\boldsymbol{\mu}_r(\mathbf{x})S_r(\mathbf{x}). \quad (2.54)$$

Suppose the material is again ergodic and statistically homogeneous. Then, individual terms in Eq. (2.54) simplify such that

$$\overline{\mathbf{M}} = \sum_{r=1}^{n} \mathbf{M}_r c_r, \qquad \overline{\boldsymbol{\gamma}(\mathbf{x})} = \sum_{r=1}^{n} \boldsymbol{\gamma}_r(\mathbf{x}) c_r,$$
$$\overline{\boldsymbol{\mu}(\mathbf{x})} = \sum_{r=1}^{n} \boldsymbol{\mu}_r(\mathbf{x}) c_r. \tag{2.55}$$

Substituting Eqs. (2.53) and (2.55) into Eq. (2.52) readily provides the extended averaged form of the dual Hashin-Shtrikman principle

$$\begin{aligned}
\overline{U}\boldsymbol{\gamma} = \frac{1}{2}\int_\Omega \boldsymbol{\Sigma} &: \boldsymbol{E}\,\mathrm{d}\mathbf{x} - \\
-\frac{1}{2}\sum_r \int_\Omega \Big(c_r(\boldsymbol{\gamma}_r(\mathbf{x}) - \boldsymbol{\mu}_r(\mathbf{x})) &: (\mathbf{M}_r - \mathbf{M}_0)^{-1} : \\
: (\boldsymbol{\gamma}_r(\mathbf{x}) - \boldsymbol{\mu}_r(\mathbf{x})) &- 2c_r\boldsymbol{\gamma}_r(\mathbf{x}) : \boldsymbol{\Sigma}\Big)\mathrm{d}\mathbf{x} + \\
+\frac{1}{2}\sum_r\sum_s \int_\Omega \boldsymbol{\gamma}_r(\mathbf{x}) &: \int_\Omega \sigma^*_{\mathbf{0}}(\mathbf{x}-\mathbf{x}') : \\
: [S_{rs}(\mathbf{x}-\mathbf{x}')\boldsymbol{\gamma}_s(\mathbf{x}') &- c_r\langle\boldsymbol{\gamma}\rangle]\,\mathrm{d}\mathbf{x}'\mathrm{d}\mathbf{x} - \\
-\frac{1}{2}\sum_r \int_\Omega c_r\boldsymbol{\gamma}_r(\mathbf{x}) &: \mathbf{M}_0^{-1} : (\boldsymbol{\gamma}_r(\mathbf{x}) - \langle\boldsymbol{\gamma}\rangle)\,\mathrm{d}\mathbf{x}.
\end{aligned} \tag{2.56}$$

In analogy with Eq. (2.33) we further admit only piecewise uniform variation of eigenstrain vector $\boldsymbol{\mu}$ and polarization strain $\boldsymbol{\gamma}$ ($\boldsymbol{\mu}_r(\mathbf{x}) = \boldsymbol{\mu}_r, \boldsymbol{\gamma}_r(\mathbf{x}) = \boldsymbol{\gamma}_r$). Next, after setting $\langle\boldsymbol{\gamma}\rangle = \sum_r \boldsymbol{\gamma}_r c_r$ and performing variation with respect to $\boldsymbol{\gamma}_r$ we arrive at the extended form of the stationarity conditions

$$\begin{aligned}
&\left[(\mathbf{M}_r - \mathbf{M}_0)^{-1} + \mathbf{M}_0^{-1}\right] : \boldsymbol{\gamma}_r(\mathbf{x}) c_r - \\
&\sum_{s=1}^{n} \int_\Omega \left\{\sigma^*_{\mathbf{0}}(\mathbf{x}-\mathbf{x}')\left[S_{rs}(\mathbf{x}-\mathbf{x}') - c_r c_s\right] + \mathbf{M}_0^{-1} c_r c_s\right\} : \\
&: \boldsymbol{\gamma}_s(\mathbf{x}')\mathrm{d}\mathbf{x}' = \boldsymbol{\Sigma} c_r + (\mathbf{M}_r - \mathbf{M}_0)^{-1}\boldsymbol{\mu}_r(\mathbf{x}) c_r,
\end{aligned} \tag{2.57}$$

for $r = 1, 2, \ldots, n$. Using again the engineering notation we get, in analogy with Eq. (2.33),

$$\begin{aligned}
\sum_{s=1}^{n} \Big(&\delta_{rs} c_r \left(([\mathsf{M}_r] - [\mathsf{M}_0])^{-1} + [\mathsf{M}_0]^{-1}\right) - c_r c_s\,[\mathsf{M}_0]^{-1} \\
&- [\mathsf{B}_{rs}]\Big)\{\gamma_s\} = c_r\{\Sigma\} + c_r([\mathsf{M}_r] - [\mathsf{M}_0])^{-1}\{\mu_r\},
\end{aligned} \tag{2.58}$$

where evaluation of the microstructure-dependent matrices $[\mathsf{B}_{rs}]$ is again outlined in Appendix A.
Similarly to Eqs. (2.35) and (2.36) we write after symbolic inversion of Eq. (2.58) the desired components of the polarization tensor $\boldsymbol{\gamma}_r$ in the form

$$\{\gamma_r\} = \sum_{s=1}^{n} c_s\,[\mathsf{R}_{rs}]\left(\{\Sigma\} + ([\mathsf{M}_s] - [\mathsf{M}_0])^{-1}\{\mu_s\}\right), \tag{2.59}$$

and finally

$$\{\overline{\gamma}\} = \sum_{r=1}^{n}\sum_{s=1}^{n} c_r c_s\,[\mathsf{R}_{rs}]\left(\{\Sigma\} + ([\mathsf{M}_s] - [\mathsf{M}_0])^{-1}\{\mu_s\}\right). \tag{2.60}$$

The macroscopic constitutive law is now given by

$$\{\mathsf{E}\} = \left[\mathsf{M}^{\mathsf{HS}}\right]\{\Sigma\} + \{\Upsilon^{\mathsf{HS}}\}, \tag{2.61}$$

with

$$\begin{aligned}
\left[\mathsf{M}^{\mathsf{HS}}\right] &= [\mathsf{M}_0] + \sum_{r=1}^{n}\sum_{s=1}^{n} c_r c_s\,[\mathsf{R}_{rs}], \\
\{\Upsilon^{\mathsf{HS}}\} &= \sum_{r=1}^{n}\sum_{s=1}^{n} c_r c_s\,[\mathsf{R}_{rs}]\,([\mathsf{M}_s] - [\mathsf{M}_0])^{-1}\{\mu_s\}
\end{aligned} \tag{2.62}$$

2.4. Numerical results

To make comparisons with the finite element approach and to motivate the analysis in the viscoelastic range we consider afresh the graphite fiber tow of Fig. 2(b). The primary goal is to recover the effective thermo-elastic properties already derived in [ZS01] and [SZS00].
Starting with the primary H-S variational principle, Section 2.2, the thermo-elastic macroscopic constitutive law receives the form

$$\begin{aligned}
\{\Sigma\} &= \left[\mathsf{L}^{\mathsf{HS}}\right]\{\mathsf{E}\} + \{\Lambda^{\mathsf{HS}}\} \\
&= \left[\mathsf{L}^{\mathsf{HS}}\right]\left(\{\mathsf{E}\} - \{\mathsf{m}^{\mathsf{HS}}\}\Delta\theta\right),
\end{aligned} \tag{2.63}$$

where $\{\mathsf{m}^{\mathsf{HS}}\}$ is the overall thermal strain vector of the expansion coefficients; $\left[\mathsf{L}^{\mathsf{HS}}\right]$ and $\{\Lambda^{\mathsf{HS}}\}$ follow from Eqs. (2.38) and (2.39), respectively. Note that the actual values depend on the choice of matrix $[\mathsf{L}_0]$. In particular, having properly chosen components of the stiffness matrix of the comparison medium $[\mathsf{L}_0]$ we may arrive either at the lower or upper bound on elastic stiffnesses of heterogeneous media (in the sense of quadratic forms), while intermediate values render estimates of effective stiffness matrix [DS99]. In particular, we select $[\mathsf{L}_0]$ as an artificial material with coefficients $[\mathsf{L}_0]_{ij} \overset{<}{>} [\mathsf{L}_r]_{ij}$ smallest (largest) of all $[\mathsf{L}_r]_{ij}$ in Ω.
The results appear in Table 3. Material properties of individual phases are taken from Table 2. The FFT combined with a suitable integration procedure is

phase	E_A [GPa]	E_T [GPa]	G_T [GPa]	ν_A	α_A [K^{-1}]	α_T [K^{-1}]
fiber	386	7.6	2.6	0.41	-1.2×10^{-6}	7×10^{-6}
matrix	5.5	5.5	1.96	0.40	2.4×10^{-5}	2.4×10^{-5}

Table 2: Material properties of T30/Epoxy system

Bitmap	L_{11}			L_{22}			L_{33}		
resolution	LB	FEM	UB	LB	FEM	UB	LB	FEM	UB
244×179	10.759	10.762	10.772	10.716	10.725	10.727	2.211	2.215	2.216
488×358	10.755	10.762	10.766	10.712	10.725	10.722	2.210	2.215	2.215
976×716	10.754	10.762	10.765	10.711	10.725	10.721	2.210	2.215	2.215

Table 3: Effective elastic stiffnesses [GPa]

used to evaluate the microstructure dependent matrices $[\mathsf{A}_{\mathsf{rs}}]$ (details are given in Appendix A) [2]. The thermal strain coefficients are obtained in the similar way from the overall eigenstress $\{\Lambda^{\mathsf{HS}}\}$. In particular, the overall thermal strain $\{\mathsf{m}^{\mathsf{HS}}\}$ then follows from

$$\{\mathsf{m}^{\mathsf{HS}}\} = -\left[\mathsf{L}^{\mathsf{HS}}\right]^{-1}\{\Lambda^{\mathsf{HS}}\}, \tag{2.64}$$

The results are summarized in Table 4.

If the stress control is applied the dual variational principle Eq. (2.48) can be invoked to derive the coefficients of the compliance matrix $\left[\mathsf{M}^{\mathsf{HS}}\right]$ from Eq. (2.62). Similarly to the strain control, selecting the individual entries of the compliance matrix $[\mathsf{M}_0]$ allow us to obtain either the lower or upper bound on the effective elastic compliance matrix of a heterogeneous medium. In particular, we select $[\mathsf{M}_0]$ as an artificial material with coefficients $[\mathsf{M}_0]_{ij} \overset{<}{>} [\mathsf{M}_{\mathsf{r}}]_{ij}$ smallest (largest) of all $[\mathsf{M}_{\mathsf{r}}]_{ij}$ in Ω. Results are stored in Table 5.

Eq. (2.62) can be further used to directly provide the overall coefficients of thermal expansion. As expected, they were found identical with those derived from the primary variational principle. Similar agreement between elastic stiffnesses and compliances is evident from Table 6. Letters P and D in Table 6 stand for the primary and dual variational principles, respectively, and IP denotes the results obtained from the primary variational principle when assuming the statistically isotropic material.

Clearly, the finite element solutions fall within individual bounds provided by the Hashin-Shtrikman variational principles. Tables 3 and 4 further demonstrate insensitivity of the solution to the selected bitmap resolution, as long as the volume fraction of the inclusion is the same. In addition, attributed to the assumed statistical homogeneity, the results confirm a slight anisotropy of the present medium. In terms of computer time, the efficiency of the present approach when compared to the FEM analysis is obvious. Nevertheless, to fully accept this method a number of other numerical assessment, particularly for more complex material behavior, are needed.

[2] The UB and LB columns in Tables 3–6 correspond to the lower bound (the matrix $[\mathsf{L}_0]$ with the smallest entries) and to the upper bound (the matrix $[\mathsf{L}_0]$ selected with the largest entries), respectively.

3. MATERIAL MODEL FOR POLYMERS

As suggested by the title one of the objectives here is to study the nonlinear material response of polymer matrix based composites. As an example we select a graphite/epoxy material system. The fiber is assumed to remain elastic during deformation so that the inelastic effects are limited to the matrix phase. For the composite structure plotted in Fig. 1 the PR100/2+EM100E epoxy is used as a bonding agent. An experimental program carried out on this type of material [VS03] demonstrates a relevant rate dependent response of the epoxy well described by the generalized Leonov model. Although some experimental observations advocate a pressure dependent behavior of such materials [KL97] the present approach assumes negligible volume deformation during plastic flow, which leads to a standard Mises-like formulation.

3.1. Leonov model

Combing the Eyring flow model for the plastic component of the shear strain rate

$$\frac{\mathrm{d}e_p}{\mathrm{d}t} = \frac{1}{2A}\sinh\frac{\tau}{\tau_0}, \tag{3.1}$$

Bitmap	$\alpha_x \times 10^5$			$\alpha_y \times 10^5$			$\alpha_z \times 10^7$			c_f
resolution	LB	FEM	UB	LB	FEM	UB	LB	FEM	UB	
244×179	2.271	2.269	2.281	2.246	2.248	2.254	-7.463	-7.463	-7.468	0.436
488×358	2.267	2.269	2.275	2.244	2.248	2.250	-7.461	-7.463	-7.465	0.436
976×716	2.267	2.269	2.275	2.243	2.248	2.249	-7.460	-7.463	-7.464	0.436

Table 4: Effective coefficients of thermal expansion $[\mathrm{K}^{-1}]$

Bitmap	M_{11}			M_{22}			M_{33}		
resolution	LB	FEM	UB	LB	FEM	UB	LB	FEM	UB
244×179	1.4293	1.4307	1.4312	1.4312	1.4325	1.4330	4.5168	4.52115	4.5235
488×358	1.4298	1.4307	1.4317	1.4316	1.4325	1.4334	4.5182	4.52115	4.5246
976×716	1.4298	1.4307	1.4318	1.4317	1.4325	1.4334	4.5185	4.52115	4.5250

Table 5: Effective elastic compliances [GPa^{-1}] $\times 10^{-4}$

with the elastic shear strain rate $\mathrm{d}e_e/\mathrm{d}t$ yields the one-dimensional Leonov constitutive model [Leo76]

$$\frac{\mathrm{d}e}{\mathrm{d}t} = \frac{\mathrm{d}e_e}{\mathrm{d}t} + \frac{\mathrm{d}e_p}{\mathrm{d}t} = \frac{\mathrm{d}e_e}{\mathrm{d}t} + \frac{\tau}{\eta(\mathrm{d}e_p/\mathrm{d}t)}, \tag{3.2}$$

where the shear-dependent viscosity η is provided by

$$\eta(\mathrm{d}e_p/\mathrm{d}t) = \frac{\eta_0 \tau}{\tau_0 \sinh(\tau/\tau_0)} = \eta_0 a_\sigma(\tau). \tag{3.3}$$

In Eq. (3.1), A and τ_0 are material parameters; a_σ that appears Eq. (3.3) is the stress shift function with respect to the zero shear viscosity η_0 (viscosity corresponding to an elastic response). Clearly, the phenomenological representation of Eq. (3.2) is the Maxwell model with the variable viscosity η.

To describe multi-dimensional behavior of the material, the generalized compressible Leonov model, equivalent to the generalized Maxwell chain model, can be used [Ter96]. The viscosity term corresponding to the μ-th unit receives the form

$$\eta_\mu = \eta_{0,\mu} a_\sigma(\tau_{\mathrm{eq}}), \tag{3.4}$$

where the equivalent shear stress τ_{eq} is provided by

$$\tau_{\mathrm{eq}} = \sqrt{\frac{1}{2} s_{ij} s_{ij}}, \tag{3.5}$$

and s_{ij} is the stress deviator tensor. Admitting only small strains and isotropic material, a set of constitutive equations defining the generalized compressible Leonov model can be written as

$$\sigma_m = K\varepsilon_v, \tag{3.6}$$

$$\frac{\mathrm{d}\boldsymbol{s}}{\mathrm{d}t} = \sum_{\mu=1}^{M} 2G_\mu \left(\frac{\mathrm{d}\boldsymbol{e}}{\mathrm{d}t} - \frac{\mathrm{d}\boldsymbol{e}_{p,\mu}}{\mathrm{d}t} \right), \tag{3.7}$$

$$\boldsymbol{s}_\mu = 2\eta_\mu \frac{\mathrm{d}\boldsymbol{e}_{p,\mu}}{\mathrm{d}t} = 2\eta_{0,\mu} a_\sigma(\tau_{\mathrm{eq}}) \frac{\mathrm{d}\boldsymbol{e}_{p,\mu}}{\mathrm{d}t}, \tag{3.8}$$

$$\boldsymbol{s} = \sum_{\mu=1}^{M} \boldsymbol{s}_\mu, \tag{3.9}$$

where σ_m is the mean stress, ε_v is the volumetric strain, K is the bulk modulus and G_μ is the shear modulus of the μ-th unit.

3.2. Numerical implementation

In classical uncoupled multi-scale computational homogenization the analysis assumes separate solutions of the boundary value problems carried out at individual scales and linked such that the solution of one serves as the input for the other. Since the present contribution is concerned with the analysis on microscale it requires the solution derived on meso-scale to be passed on in form of the applied load increment as an input. For the composite geometry in Fig. 1(b) such data are usually derived using the finite element method [Wie00]. In standard displacement based formulation the primary variable supplied to micro-scale is an increment of the mesoscopic overall strain at a given integration point found for a given increment of the macroscopic load. Such loading conditions thus fit well with the primary Hashin-Shtrikman variational principle addressed in Section 2. Some specifics of the principle pertinent to the nonlinear viscoelastic response of the matrix phase will be now given.

Bitmap resolution	IP-LB L_{11}	P-LB L_{11}	D-LB M_{11}^{-1}	P-UB L_{11}	D-UP M_{11}^{-1}	IP-UB L_{11}	IP-LB L_{33}	P-LB L_{33}	D-LB M_{33}^{-1}	P-UB L_{33}	D-UP M_{33}^{-1}	IP-UB
244×179	10.744	10.759	10.759	10.772	10.772	10.754	2.211	2.211	2.213	2.216	2.216	2.214
488×358	10.744	10.755	10.755	10.766	10.766	10.754	2.211	2.210	2.210	2.215	2.215	2.214
976×716	10.744	10.754	10.754	10.765	10.765	10.754	2.211	2.210	2.210	2.215	2.215	2.214

Table 6: Comparison of primary and dual principles

To extend the class of problems represented by Eqs. (2.37), (2.61) beyond the thermo-elastic response we examine the overall behavior and local fields in a fibrous composite system in Fig. 2 assuming elastic-nonlinear viscoelastic phases. Introducing nonlinear effects requires to write Eq. (2.37) in the incremental form as

$$\{\Delta\Sigma(t_i)\} = \left[\mathsf{L}^{\mathsf{HS}}(t_i)\right]\{\Delta\mathsf{E}\} + \{\Delta\Lambda^{\mathsf{HS}}(t_i)\}, \quad (3.10)$$

where $\left[\mathsf{L}^{\mathsf{HS}}(t_i)\right]$ represents the instantaneous stiffness matrix at a time instant t_i derived from Eq. (2.37) and $\{\Delta\Lambda^{\mathsf{HS}}(t_i)\}$ is the current increment of the mesoscopic eigenstress Eq. (2.37) that stores contribution due to nonlinear viscoelastic response. The local counterparts of Eq. (3.10) are provided by

$$\begin{aligned} \{\Delta\sigma_{\mathsf{f}}\} &= [\mathsf{L}_{\mathsf{f}}]\{\Delta\varepsilon_{\mathsf{f}}\}, & (3.11)\\ \{\Delta\sigma_{\mathsf{m}}(t_i)\} &= \left[\mathsf{L}_{\mathsf{m}}(K,\widehat{G}(t_i)\right]\{\Delta\varepsilon_{\mathsf{m}}\} + \\ &+ \{\Delta\lambda_{\mathsf{m}}(t_i)\}, & (3.12)\end{aligned}$$

where in accordance with our assumption $[\mathsf{L}_{\mathsf{f}}]$ stands for the time independent elastic stiffness matrix of the fiber phase with no viscoelastic contribution to the overall local strain. The instantaneous stiffness matrix of the matrix phase $\left[\mathsf{L}_{\mathsf{m}}(K,\widehat{G}(t_i)\right]$, however, evolves with time and is written in terms of the time independent bulk modulus K and the instantaneous time dependent shear modulus $\widehat{G}(t_i)$. Together with the matrix eigenstress increment $\{\Delta\lambda_{\mathsf{m}}(t_i)\}$ it follows from a suitable integration procedure applied to the set of Eqs. (3.6)-(3.9).

Fully implicit integration scheme

To avoid possible numerical instabilities linked to explicit integration schemes a fully implicit Euler backward integration procedure is developed. Providing the total strain rate is constant during integration a new state of stress in the matrix phase at the end of the current time step assumes the form (subscript m, identifying the matrix phase, is dropped from subsequent equations)

$$\begin{aligned} \sigma_m(t_i) &= \sigma_m(t_{i-1}) + K\Delta\varepsilon_v, & (3.13)\\ \{\mathsf{s}(t_i)\} &= \{\mathsf{s}(t_{i-1})\} + \\ &+ 2\widehat{G}(t_i)\,[\mathsf{Q}]\,\{\Delta\mathsf{e}\} + \{\Delta\lambda(t_i)\}, & (3.14)\end{aligned}$$

where t_i is the current time at the end of the i-th time increment; $\sigma_m(t_i)$ is the elastic means stress, $\{\mathsf{s}(t_i)\}$ stores the deviatoric part of the stress vector $\{\Delta\sigma(t_i)\}$ and $\{\Delta\mathsf{e}\}$ is the deviatoric part of the total strain increment. With reference to the backward Euler integration scheme the time dependent variables at time instant t_i receive the form

$$\widehat{G}(t_i) = \sum_{\mu=1}^{M} G_\mu \frac{\theta_\mu a_\sigma(t_i)}{\Delta t}\left(1-\exp\left(-\frac{\Delta t}{\theta_\mu a_\sigma(t_i)}\right)\right), \quad (3.15)$$

$$\{\Delta\lambda(t_i)\} = -\sum_{\mu=1}^{M}\left(1-\exp\left(-\frac{\Delta t}{\theta_\mu a_\sigma(t_i)}\right)\right)\{\mathsf{s}_\mu(t_{i-1})\}, \quad (3.16)$$

where G_μ represents the elastic shear modulus in the μ-th unit of the Maxwell chain model, θ_μ is the associated relaxation time, $\{\mathsf{s}_\mu(\mathsf{t_i})\}, \mu = 1,2,\ldots,M$, is the deviatoric stress vector in individual units evaluated at the beginning of a new time increment $\Delta t = t_i - t_{i-1}$, and M is the assumed number of Maxwell units in the chain model; $a_\sigma(t_i)$ is the stress shift factor given by

$$a_\sigma(t_i) = \frac{\tau_{eq}(t_i)}{\tau_0}/\sinh\frac{\tau_{eq}(t_i)}{\tau_0}, \quad (3.17)$$

where the equivalent stress $\tau_{eq}(t_i)$ follows from

$$\tau_{eq}(t_i) = \sqrt{\frac{1}{2}\{\mathsf{s}(t_i)\}^{\mathsf{T}}\,[\mathsf{Q}]^{-1}\,\{\mathsf{s}(t_i)\}}, \quad (3.18)$$

and

$$[\mathsf{Q}] = \mathrm{diag}\left[1,1,1,\frac{1}{2},\frac{1}{2},\frac{1}{2}\right]. \quad (3.19)$$

Clearly, the backward Euler step makes all variables nonlinearly dependent on the end stress values found at time t_i. Therefore, a successful completion of a given integration step requires the solution of a system of nonlinear equations. Here, the solution is established employing the Newton-Raphson method. To that end, define a set of residuals $\{\mathsf{r}\} = \{T, G, A\}^{\mathsf{T}}$ as

$$\begin{aligned} T &= \tau_{eq}(t_i) - \sqrt{\frac{1}{2}\{\mathsf{s}(t_i)\}^{\mathsf{T}}\left[\mathsf{Q}\right]^{-1}\{\mathsf{s}(t_i)\}}, \\ G &= \widehat{G}(t_i) - \\ &- \sum_{\mu=1}^{M} G_\mu \frac{\theta_\mu a_\sigma(t_i)}{\Delta t}\left(1 - \exp\left(-\frac{\Delta t}{\theta_\mu a_\sigma(t_i)}\right)\right), \\ A &= a_\sigma(t_i) - \frac{\tau_{eq}(t_i)}{\tau_0}/\sinh\frac{\tau_{eq}(t_i)}{\tau_0}, \end{aligned}$$

with

$$\{\mathsf{a}\} = \{\tau_{eq}(t_i), \widehat{G}(t_i), a_\sigma(t_i)\}^{\mathsf{T}}, \tag{3.20}$$

being the primary variables. Note that the current increment of the eigenstress vector $\{\Delta\lambda(t_i)\}$ that appears in Eq. (3.14) is considered as a secondary variable. Under the condition that $\{\Delta\mathsf{e}\}$ is constant the Newton-Raphson iterative scheme reads

$$\{\mathsf{a}\}^{k+1}(t_i) = \{\mathsf{a}\}^{k}(t_i) - \left[\mathsf{H}\right]^{-1}\{\mathsf{r}\}^{k}, \tag{3.21}$$

where the Jacobian matrix $[\mathsf{H}]$ is given by

$$\left[\mathsf{H}\right] = \begin{bmatrix} \frac{\partial T}{\partial \tau_{eq}} & \frac{\mathrm{d}T}{\mathrm{d}\widehat{G}} & \frac{\mathrm{d}T}{\mathrm{d}a_\sigma} \\ \frac{\partial G}{\partial \tau_{eq}} & \frac{\partial G}{\partial \widehat{G}} & \frac{\partial G}{\partial a_\sigma} \\ \frac{\partial A}{\partial \tau_{eq}} & \frac{\partial A}{\partial \widehat{G}} & \frac{\partial A}{\partial a_\sigma} \end{bmatrix}. \tag{3.22}$$

The total differentials in matrix $[\mathsf{H}]$ follow from the chain rule

$$\frac{\mathrm{d}T}{\mathrm{d}\widehat{G}} = \frac{\partial T}{\partial \widehat{G}} + \left\{\frac{\partial T}{\partial \Delta\lambda}\right\}^{\mathsf{T}}\left\{\frac{\partial \Delta\lambda}{\partial \widehat{G}}\right\}, \tag{3.23}$$

$$\frac{\mathrm{d}T}{\mathrm{d}a_\sigma} = \left\{\frac{\partial T}{\partial \Delta\lambda}\right\}^{\mathsf{T}}\left\{\frac{\partial \Delta\lambda}{\partial a_\sigma}\right\}. \tag{3.24}$$

The initial values of primary variables at time t_i for $k = 0$ are set to forward Euler estimates. Once the time dependent variables are known at time t_i the updated stress vectors $\{\mathsf{s}_\mu(\mathsf{t_i})\}$ is found from

$$\begin{aligned} \{\mathsf{s}_\mu(t_i)\} &= \{\mathsf{s}_\mu(t_{i-1})\}\exp\left(\frac{-\Delta t}{\theta_\mu a_\sigma(t_i)}\right) + \\ &+ 2G_\mu\frac{\theta_\mu a_\sigma(t_i)}{\Delta t}\times \\ &\times \left(1 - \exp\left(-\frac{\Delta t}{\theta_\mu a_\sigma(t_i)}\right)\right)\left[\mathsf{Q}\right]\{\Delta\mathsf{e}\}. \end{aligned} \tag{3.25}$$

The above approach is used in Section 4 to derive the results for the selected example problems. In addition, comparisons with fully explicit integration scheme printed in one-dimensional format further highlight the superiority of the backward Euler method that allows for a substantially longer time increment with no signs of oscillations, see Appendix B for more refined discussion.

4. NUMERICAL EXAMPLES

To illustrate the proposed procedure, we examined the time dependent response of the material system addressed already in Section 2.4. Note that the material properties listed in Table 2 correspond to the graphite fibers and PR100/2+EM100E epoxy matrix. The parameters of the Leonov model were determined from a set of creep experiments performed at various stress levels. Ten elements of the generalized Kelvin-Voight chain model were used to obtain an accurate description of the linear compliance function. Laplace transform was then used to invert the creep compliance function (see [VS03] for more details). The resulting coefficients needed in the generalized Maxwell chain model appear in Table 7.

Parameter	***Value***	
A [s]	4.854×10^{14}	
τ_0 [MPa]	1.57	
K [MPa]	5030	
μ	θ_μ [MPa·s]	G_μ [MPa]
1	1.4664×10^{1}	1.1479×10^{0}
2	1.0194×10^{3}	1.0293×10^{1}
3	2.4024×10^{4}	2.4589×10^{1}
4	2.7624×10^{5}	2.8396×10^{1}
5	2.9746×10^{6}	3.0671×10^{1}
6	4.6200×10^{7}	4.2446×10^{1}
7	4.7063×10^{8}	4.9675×10^{1}
8	5.7611×10^{9}	6.1870×10^{1}
9	8.9183×10^{10}	1.0178×10^{2}
10	7.2765×10^{13}	7.2765×10^{2}

Table 7: Nonlinear viscoelastic material properties of PR100/2+EM100E epoxy matrix

As indicated in the previous sections, only the loading due to constant overall strain rate is considered and the analysis is again carried out assuming generalized plane strain. Also, based on the results derived for linear viscoelasticity [SZ02b], the reference stiffness matrix $[\mathsf{L}_0]$ is selected as the smallest of all $[\mathsf{L}_\mathsf{r}]_{ij}$.

First, the sensitivity of the overall response with respect to the choice of the reference stiffness matrix $[\mathsf{L}_0]$ is analyzed. To study this influence, the ratio $|1 - \widehat{G}(t_i)/\widehat{G}_{\rm ref}|$ was used to control the update of the reference medium. If this ratio exceeded a given tolerance ξ, the reference value $\widehat{G}_{\rm ref}$ was set to $\widehat{G}(t_i)$, the reference stiffness matrix $[\mathsf{L}_0]$ was accordingly modified and the associated microstructural matrices were reevaluated. Since this is just a test study, the results that appear in Fig. 6 were derived for a statistically isotropic microstructure with the same fiber volume fraction as the original material. Apparently, the H-S based procedure is rather insensitive to updating tolerance; to get practically indistinguishable overall response it suffices to set $\xi = 0.01$.

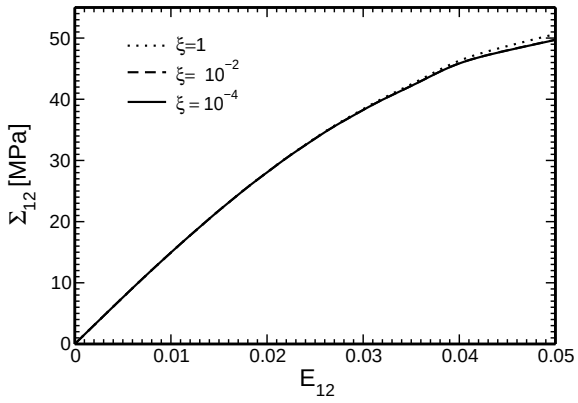

Figure 6: Sensitivity with respect to reference medium update, hexagonal packing for $\dot{E}_{12} = 10^{-4}\,\mathrm{s}^{-1}$

Next, an effect of a bitmap resolution on the overall response of the real, statistically *non-isotropic*, composite material system is addressed. Similarly to the thermoelasticity case, the results displayed in Fig. 7 again demonstrate the insensitivity of the overall response to a bitmap resolution; in particular, the bitmap with dimensions 488×358 pixels gives results identical to the highest resolution 976×716 pixels for both E_{11} and E_{12} loading.

The next set of figures, Figs. 8(a,b), shows the overall response for various overall transverse and shear strain rates. Evidently, the overall response of the composite is almost rate independent for the E_{11} loading. This is attributed to the fact that the response is governed by elastic fibers while the shear stresses in matrix remain too low to trigger the plastic flow. The results found for the shear loading E_{12}, however, demonstrate the ability of the H-S based approach to correctly represent the rate dependent response of the matrix phase.

Finally, for the sake of completeness, the slightly anisotropic character of the examined material system already suggested by thermoelastic analysis, Table 3, is demonstrated by plotting phase stresses due to E_{11} and E_{22} loading, see Figs. 9(a) and 9(b). This result cannot be obtained when using statistically isotropic microstructures, as typically done in analytical modeling approaches.

5. CONCLUSIONS

Homogenized mesoscopic response of fiber tow with disordered distribution of graphite fibers in the epoxy matrix was analyzed for loading conditions that promote evolution of local eigenstresses or eigenstrains. Contributions due to thermal and nonlinear viscoelastic effects were considered. The homogenized (effective) response of the composite system was found with the help of the Hashin-Shtrikman variational principles that make possible to account, at least to some extend, for a typical random character of real microstructures by introducing the low order statistical descriptors such as the one- and two-point probability functions into their formulation.

Color images of real microstructure, obtained by scanning electron microscope and converted into their binary counterparts using the image analyzer LUCIA, were used to evaluate the desired statistical descriptors. To that end, a fairly efficient procedure that combines the knowledge of a real microstructure given in a binary form with a Discrete Fourier Transform of individual variables was implemented. Note that only representation of the two-point probability function in the Fourier space is needed for the evaluation of microstructure dependent matrices $[\mathsf{A}_{\rm rs}]$ and $[\mathsf{A}_{\rm rs}]$, Eqs. (A.13)-(A.14). Such a representation readily admits selection of a generally anisotropic comparison medium, which usually arises in estimation of bounds, recall Eqs. (A.4)-(A.9).

In this framework, both the primary and dual variational principles were revisited to provide bounds on elastic and thermal properties of a selected material system assuming statistically uniform distribution of reinforcements. As expected, both the displacement and traction boundary conditions can be employed to deliver the same results as shown in Table 6. The results presented in Tables 3, 4 and 5 further suggest a slight anisotropy of the present medium, which cannot be captured when simply as-

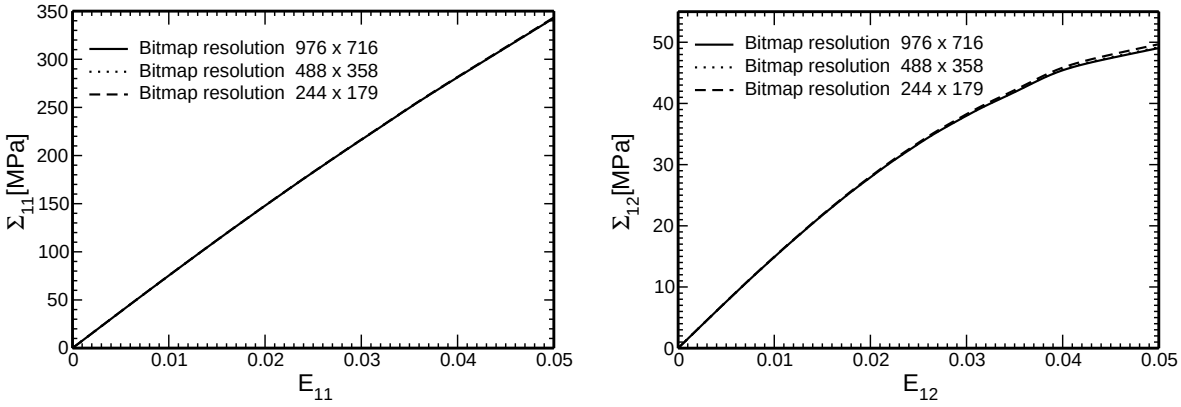

(a) (b)

Figure 7: Effect of a bitmap resolution (a) $\dot{E}_{11} = 10^{-4}$ s^{-1}, (b) $\dot{E}_{12} = 10^{-4}$ s^{-1}

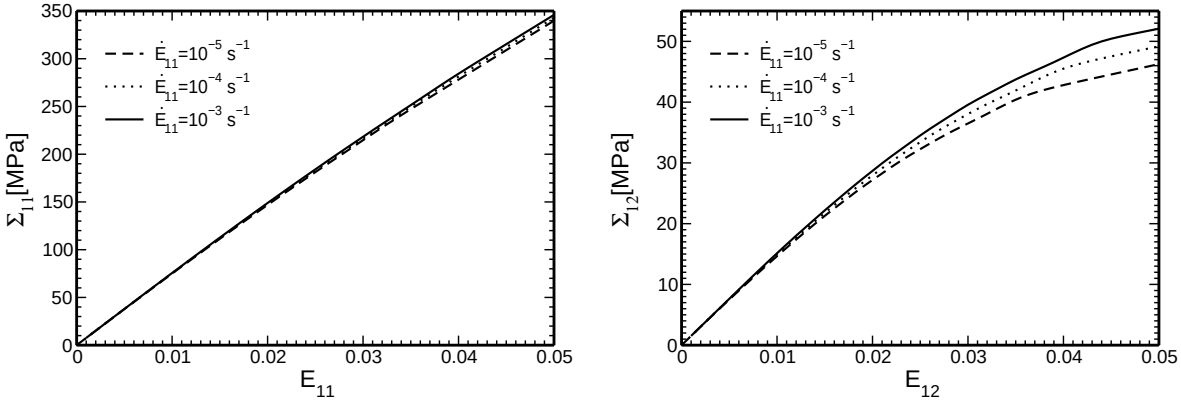

(a) (b)

Figure 8: Overall response, (a) $\dot{E}_{11}$ loading, (b) $\dot{E}_{12}$ loading.

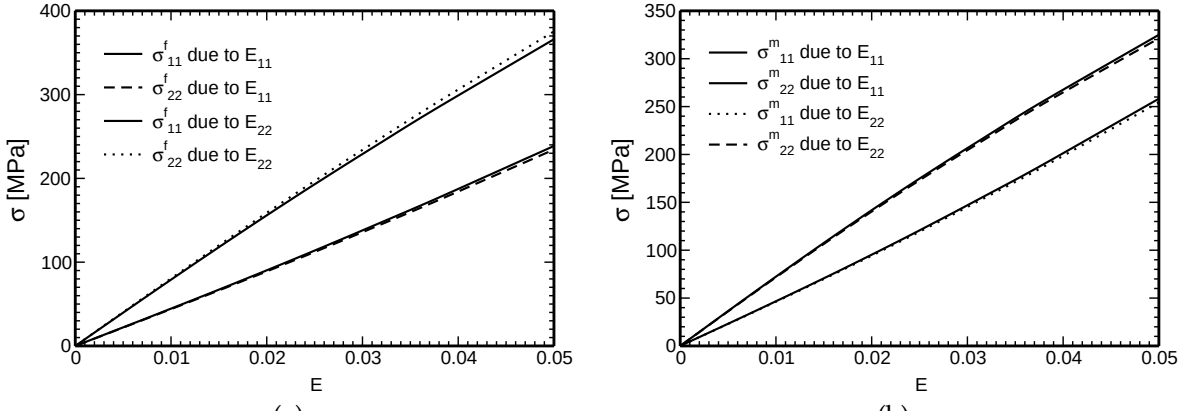

(a) (b)

Figure 9: Local response (a) Fiber phase, (b) Matrix phase

suming a statistical isotropy of a medium. This is also supported by the results derived from the finite element analysis on periodic unit cells, [ZS01].

In the context of initial stresses this methodology was extended to treat nonlinear effects. In particular, the nonlinear viscoelastic response of the matrix phase governed by the generalized Leonov model was examined. The results suggest essentially a linear behavior when loading the composite by E_{11} or E_{22} components of the overall strain. The rate dependent behavior, however, was confirmed for loading conditions that activate yielding in the matrix phase, Figs. 8. Figs. 9 further confirm a slight anisotropy already reported for the effective elastic moduli. More pronounced difference in the directional response is expected for material systems with higher material contrast in the transverse elastic moduli of the two phases.

To enhance efficiency and stability of numerical analysis, the integration of time dependent matrices is implemented in the fully implicit format. The expected advantages of this technique over the fully explicit approach are demonstrated in Appendix B on a simple one-dimensional problem.

In summary, the use of the Hashin-Shtrikman variational principles should considerably speed up the micromechanical analysis at least on the level of constituents thus enhance the overall efficiency of large multi-scale calculations. Although applications of averaging techniques on mesoscale (woven composites) received some attention, their use in nonlinear environment is questionable.

Acknowledgments

Financial support was provided partially by the GAČR grants No. 106/03/0180, No. 103/01/D052 and partially by research projects MSM 210000001,3.

A. EVALUATION OF MATRICES $[\mathsf{A}_{rs}]$ AND $[\mathsf{B}_{rs}]$

A.1. The Fourier transform of tensors ϵ_0^* and σ_0^*

In Section 2 we introduced the fourth order tensor $(\epsilon_0^*)_{ijkl}$ related to the fundamental solution $(u_0^*)_{ij}$. Specific forms of these quantities for a homogeneous and isotropic material and certain special cases of anisotropic materials can be found, e.g., in [BS96, Mur87]. Their Fourier transforms, however, needed for evaluation of matrices $[\mathsf{A}_{rs}]$ and $[\mathsf{B}_{rs}]$ in Eqs. (2.34) and (A.14), deserve more attention.

First, consider the tensor $(\epsilon_0^*)_{ijkl}$ derived by differentiating the so-called *fundamental solution* u_{pi}^* that satisfies the Lamé equation

$$(L_0)_{ijkl}(u_0^*)_{pk,lj}(\mathbf{x}-\mathbf{x}') + \delta_{pi}\delta(\mathbf{x}-\mathbf{x}') = 0, \quad \text{(A.1)}$$

It represents the displacements in the i direction at a point $\mathbf{x}$ due to a unit point force applied at a point $\mathbf{x}'$ in the direction p. Similarly, tensor ϵ_{pij}^* given by

$$(\epsilon_0^*)_{pij} = \frac{1}{2}((u_0^*)_{pi,j} + (u_0^*)_{pj,i}), \quad \text{(A.2)}$$

then corresponds to the strains at a point $\mathbf{x}$ due to a unit point force applied at a point $\mathbf{x}'$ in the p^{th} direction. As shown in, e.g., [Krö86, Wil77], the fourth order tensor $(\epsilon_0^*)_{ijkl}$ follows directly by differentiating Eq. (A.2).

$$(\epsilon_0^*)_{ijkl}(\mathbf{x}) = \frac{1}{4}\Big((u_0^*)_{ik,lj}(\mathbf{x}) + (u_0^*)_{il,kj}(\mathbf{x}) + \\ + (u_0^*)_{jk,li}(\mathbf{x}) + (u_0^*)_{jl,ki}(\mathbf{x})\Big). \quad \text{(A.3)}$$

Hence, according to definition, the Fourier transform of Eq. (A.3) can be written in the form

$$\widetilde{(\epsilon_0^*)}_{ijkl}(\boldsymbol{\xi}) = -\frac{1}{4}\Big(\widetilde{(u_0^*)}_{ik}(\boldsymbol{\xi})\xi_l\xi_j + \widetilde{(u_0^*)}_{il}(\boldsymbol{\xi})\xi_k\xi_j + \\ + \widetilde{(u_0^*)}_{jk}(\boldsymbol{\xi})\xi_l\xi_i + \widetilde{(u_0^*)}_{jl}(\boldsymbol{\xi})\xi_k\xi_i\Big). \quad \text{(A.4)}$$

Similarly, the Fourier transform of Eq. (A.1) reads

$$-(L_0)_{ijkl}\xi_i\xi_l\widetilde{(u_0^*)}_{jm}(\boldsymbol{\xi}) + \delta_{km} = 0, \quad \text{(A.5)}$$

so that

$$\widetilde{(u_0^*)}_{jk}(\boldsymbol{\xi}) = ((L_0)_{ijkl}\xi_i\xi_l)^{-1}. \quad \text{(A.6)}$$

The Fourier transform of the tensor $\widetilde{(\sigma_0^*)}_{ijkl}$ is given by

$$\widetilde{(\sigma_0^*)}_{ijkl} = -(L_0)_{ijpq}\widetilde{(\epsilon_0^*)}_{pqrs}(L_0)_{rskl}. \quad \text{(A.7)}$$

The engineering form of tensors $\widetilde{(\epsilon_0^*)}_{ijkl}$ and $\widetilde{(\sigma_0^*)}_{ijkl}$ for the generalized plane strain are

$$\left[\widetilde{\epsilon_0^*}\right] = \begin{bmatrix} \widetilde{(\epsilon_0^*)}_{1111} & \widetilde{(\epsilon_0^*)}_{1122} & 2\widetilde{(\epsilon_0^*)}_{1112} & 0 \\ \widetilde{(\epsilon_0^*)}_{1122} & \widetilde{(\epsilon_0^*)}_{2222} & 2\widetilde{(\epsilon_0^*)}_{2212} & 0 \\ 2\widetilde{(\epsilon_0^*)}_{1112} & 2\widetilde{(\epsilon_0^*)}_{2212} & 4\widetilde{(\epsilon_0^*)}_{1212} & 0 \\ 0 & 0 & 0 & 0 \end{bmatrix}, \quad \text{(A.8)}$$

and

$$\left[\widetilde{\sigma_0^*}\right] = -\left[\mathsf{L}_0\right]\left[\widetilde{\epsilon_0^*}\right]\left[\mathsf{L}_0\right], \quad \text{(A.9)}$$

where the last row and column in matrix $\left[\widetilde{\epsilon_0^*}\right]$ were augmented by zeros to comply with the generalized plane strain assumption.

To make a final comment we draw the reader's attention to Eqs. (A.4) and (A.7) which suggest that the Fourier transform of $\widetilde{\epsilon_0^*}$ and $\widetilde{\sigma_0^*}$ can be easily obtained for any homogeneous anisotropic reference medium, which is not generally possible for functions ϵ_0^* and $\boldsymbol{\sigma_0^*}$.

A.2. Microstructural matrices

Consider Eq. (2.34) to write the microstructure-dependent matrices $[\mathsf{A_{rs}}]$ in the form

$$\begin{aligned}[\mathsf{A_{rs}}] &= \int_\Omega [\epsilon_0^*](\mathbf{x}-\mathbf{x}')\,(S_{rs}(\mathbf{x}-\mathbf{x}')-c_r c_s)\,\mathrm{d}\mathbf{x}' \\ &= \int_\Omega [\epsilon_0^*](\mathbf{x}-\mathbf{x}')S'_{rs}(\mathbf{x}-\mathbf{x}')\mathrm{d}\mathbf{x}' \\ &= \int_\Omega [\epsilon_0^*](\mathbf{x})S'_{rs}(\mathbf{x})\mathrm{d}\mathbf{x}, \qquad (A.10)\end{aligned}$$

where S'_{rs} denotes the fluctuating part of S_{rs} under the no-long range orders hypothesis. Next, recall the definition of the Fourier transform to observe that the preceding formula can be written as

$$\begin{aligned}[\mathsf{A_{rs}}] &= \int_\Omega [\epsilon_0^*](\mathbf{x})S'_{rs}(\mathbf{x})\mathrm{d}\mathbf{x} \\ &= \left[\int_\Omega [\epsilon_0^*](\mathbf{x})S'_{rs}(\mathbf{x})\mathrm{e}^{\mathrm{i}\mathbf{x}\cdot\boldsymbol{\xi}}\mathrm{d}\Omega(\mathbf{x})\right]_{\boldsymbol{\xi}=\mathbf{0}} \\ &= \mathcal{F}\left[[\epsilon_0^*](\mathbf{x})S'_{rs}(\mathbf{x})\right]_{\boldsymbol{\xi}=\mathbf{0}}. \qquad (A.11)\end{aligned}$$

Eq. (A.11) can be further modified to get (see [DW96])

$$\begin{aligned}[\mathsf{A_{rs}}] &= \frac{1}{(2\pi)^2}\left[\int_\Omega \widetilde{[\epsilon_0^*]}(\boldsymbol{\xi}-\boldsymbol{\xi}')\widetilde{S'}_{rs}(\boldsymbol{\xi}')\mathrm{d}\boldsymbol{\xi}'\right]_{\boldsymbol{\xi}=\mathbf{0}} \\ &= \frac{1}{(2\pi)^2}\int_\Omega \widetilde{[\epsilon_0^*]}(-\boldsymbol{\xi}')\widetilde{S'}_{rs}(\boldsymbol{\xi}')\mathrm{d}\boldsymbol{\xi}' \qquad (A.12)\end{aligned}$$

Since $\widetilde{\epsilon_0^*}(-\boldsymbol{\xi}) = \widetilde{\epsilon_0^*}(\boldsymbol{\xi})$, see Eq. (A.4), we finally arrive at

$$[\mathsf{A_{rs}}] = \frac{1}{(2\pi)^2}\int_\Omega \widetilde{[\epsilon_0^*]}(\boldsymbol{\xi}')\widetilde{S'}_{rs}(\boldsymbol{\xi}')\mathrm{d}\boldsymbol{\xi}'. \qquad (A.13)$$

Similar procedure then provides

$$[\mathsf{B_{rs}}] = \frac{1}{(2\pi)^2}\int_\Omega \widetilde{[\sigma_0^*]}(\boldsymbol{\xi}')\widetilde{S'}_{rs}(\boldsymbol{\xi}')\mathrm{d}\boldsymbol{\xi}'. \qquad (A.14)$$

Thus knowing the values of $\widetilde{S'}_{rs}$ we may evaluate integrals (A.13) and (A.14) by an appropriate numerical integration procedure.

We close this section by introducing certain universal connections for matrices $[\mathsf{A_{rs}}]$ and $[\mathsf{B_{rs}}]$ evaluated for the two-phase composite medium. In particular, recall Eq. (2.5) to write function S'_{rs} as

$$\begin{aligned}S'_{rs}(\mathbf{x},\mathbf{x}') &= \overline{\chi_r(\mathbf{x},\alpha)(\chi_s(\mathbf{x}',\alpha)-S_s(\mathbf{x}'))} \\ &= \overline{(\chi_r(\mathbf{x},\alpha)-S_r(\mathbf{x}))\chi_s(\mathbf{x}',\alpha)}. \qquad (A.15)\end{aligned}$$

The above relation together with Eq. (2.3) implies that

$$\begin{aligned}S'_{mm} &= S_{mm}-S_m^2, \\ S'_{ff} &= S_{mm}-S_m^2 = S'_{mm}, \qquad (A.16)\\ S'_{fm} &= S'_{mf}-S'_{mm}. \qquad (A.17)\end{aligned}$$

Introducing relations (A.16) into Eq. (A.10) yields

$$\begin{aligned}[\mathsf{A_{mm}}] = [\mathsf{A_{ff}}] = -[\mathsf{A_{mf}}], \\ [\mathsf{B_{mm}}] = [\mathsf{B_{ff}}] = -[\mathsf{B_{mf}}]. \qquad (A.18)\end{aligned}$$

It now becomes clear that only a single matrix, say $[\mathsf{A_{mm}}]$, needs to be evaluated numerically, which substantially decreases the computational effort. Introducing auxiliary matrices

$$\begin{aligned}[\mathsf{A}] &= [\mathsf{A_{mm}}], \\ [\mathsf{B}] &= c_m c_f\,[\mathsf{M_0}]^{-1}-[\mathsf{B_{mm}}] \\ [\mathsf{K_r}] &= [\mathsf{L_r}]-[\mathsf{L_0}], \\ [\mathsf{N_r}] &= \left(([\mathsf{M_r}]-[\mathsf{M_0}])^{-1}+[\mathsf{M_0}]^{-1}\right)^{-1}\end{aligned}$$

we can finally obtain, with the help of Eq. (A.18), the matrices $[\mathsf{T_{rs}}]$ and $[\mathsf{R_{rs}}]$ in the form

$$\begin{aligned}[\mathsf{T_{rs}}] = [\mathsf{K_r}]\left(c_f\,[\mathsf{K_m}]+c_m\,[\mathsf{K_f}]-c_f c_m\,[\mathsf{A}]^{-1}\right) \qquad (A.19)\\ \left([\mathsf{K_f}]+[\mathsf{K_m}]-[\mathsf{K_r}]+\delta_{rs}(1-c_r)\,[\mathsf{A}]^{-1}\right), \\ [\mathsf{R_{rs}}] = [\mathsf{N_r}]\left(c_f\,[\mathsf{N_m}]+c_m\,[\mathsf{N_f}]-c_f c_m\,[\mathsf{B}]^{-1}\right) \qquad (A.20)\\ \left([\mathsf{N_f}]+[\mathsf{N_m}]-[\mathsf{N_r}]+\delta_{rs}(1-c_r)\,[\mathsf{B}]^{-1}\right).\end{aligned}$$

B. NUMERICAL INTEGRATION OF THE LEONOV MODEL IN THE ONE-DIMENSIONAL SETTING

Here we present a brief comparison between the fully implicit integration scheme proposed in Section 2.4 and the fully explicit procedure with forward integration step often used in linear viscoelastic analysis. To keep the discussion simple we limit our attention to an one-dimensional problem.

To introduce the subject consider Fig. 10(a) showing a typical uniaxial response of the PR100/2+EM100E epoxy subjected to a constant tensile strain rate. The plotted curves are found for $\dot{\varepsilon}_x = 5\times10^{-3}\ \mathrm{s}^{-1}$. The

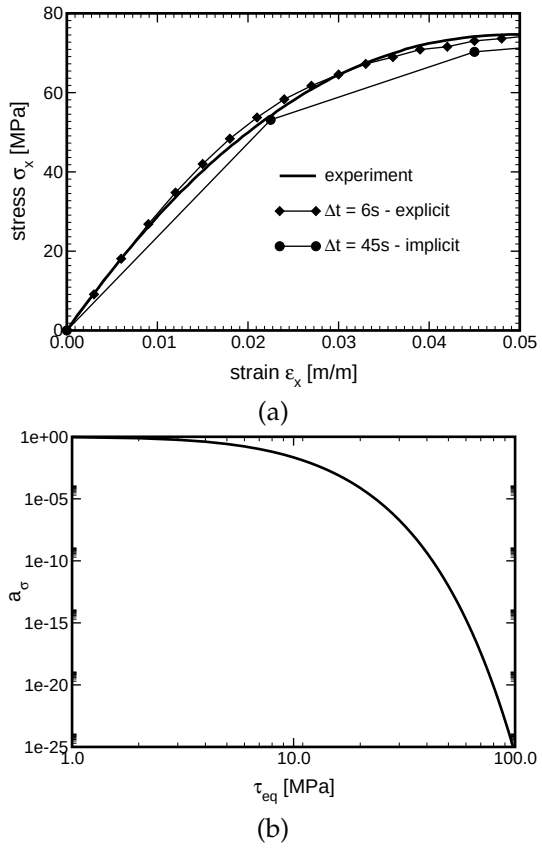

Figure 10: (a) experiment vs. numerical simulation, (b) variation of a_σ

solid line is obtained experimentally while the others follow from the numerical analysis using the two integration schemes with the largest possible time increments, for which now stability problems occurred.

Fig. 10(a) suggests that in order to avoid numerical instabilities with the explicit forward Euler method a relatively short time increment must be prescribed. This becomes clear once we recall the basic ingredient of the method, which is the assumption that all time dependent parameters are taken, for the forward integration step, from the beginning of a new time increment and are kept constant. This assumption clearly breaks down for the stress shift parameter a_σ, which is a highly nonlinear function of stress and rapidly approaches zero with increasing stress level as demonstrated in Fig. 10(b). This method, however, is extremely simple to implement and requires only a few calculations per time integration step. Nevertheless, the conditional stability may be the major obstacle in successful implementation within the framework of large multi-scale computation.

A rather different numerical response is evident for the fully implicit integration scheme. Although at a slight expense of accuracy, the stable behavior outlast even for a relatively large time step. On the other hand, a local Newton-Raphson iteration is required to arrive at correct values of the time dependent variables at the end of a given time step. While this may slow down the local integration, a significant reduction in number of required time steps may eventually prove beneficial. To complete our discussion on this subject the one-dimensional counterpart of Eqs. (3.13)-(3.18) is now given.

Equations driving the one-dimensional tensile viscoelastic response are

$$
\begin{aligned}
\sigma(t_i) &= \sigma(t_{i-1}) + \widehat{E}(t_i)\left(\Delta\varepsilon - \widehat{\varepsilon}(t_i)\right), \\
\widehat{E}(t_i) &= \sum_{\mu=1}^{M} E_\mu \frac{\theta_\mu a_\sigma(t_i)}{\Delta t} \times \\
&\times \left(1 - \exp\left(-\frac{\Delta t}{\theta_\mu a_\sigma(t_i)}\right)\right), \\
\widehat{\varepsilon}(t_i) &= \frac{1}{\widehat{E}(t_i)} \times \\
&\times \sum_{\mu=1}^{M} \left(1 - \exp\left(-\frac{\Delta t}{\theta_\mu a_\sigma(t_i)}\right)\right) \sigma_\mu(t_{i-1}), \\
\tau_{eq}(t_i) &= \frac{\sigma(t_i)}{\sqrt{3}}, \\
a_\sigma(t_i) &= \frac{\tau_{eq}(t_i)}{\tau_0} / \sinh\frac{\tau_{eq}(t_i)}{\tau_0}.
\end{aligned}
$$

The vector of residuals $\{\mathsf{r}\} = \{T, G, A\}^\mathsf{T}$ in Newton-Raphson iteration step now becomes

$$
\begin{aligned}
T &= \tau_{eq}(t_i) - \\
&- \frac{1}{\sqrt{3}}\left(\sigma(t_{i-1}) + \widehat{E}(t_i)\left(\Delta\varepsilon - \Delta\widehat{\varepsilon}(t_i)\right)\right), \\
G &= \widehat{E}(t_i) - \\
&- \sum_{\mu=1}^{M} E_\mu \frac{\theta_\mu a_\sigma(t_i)}{\Delta t}\left(1 - \exp\left(-\frac{\Delta t}{\theta_\mu a_\sigma(t_i)}\right)\right), \\
A &= a_\sigma(t_i) - \frac{\tau_{eq}(t_i)}{\tau_0} / \sinh\frac{\tau_{eq}(t_i)}{\tau_0},
\end{aligned}
$$

where the vector of unknowns receives the form

$$\{\mathsf{a}\} = \{\tau_{eq}(t_i), \widehat{E}(t_i), a_\sigma(t_i)\}^\mathsf{T}. \qquad \text{(B.1)}$$

The required derivatives that appear in the Jacobian

matrix [H], Eq. (3.21), are listed in a sequel:

$$\frac{\partial T}{\partial \tau_{eq}} = 1, \quad \frac{\mathrm{d}T}{\mathrm{d}\widehat{E}} = -\frac{\Delta\varepsilon}{\sqrt{3}}, \quad \frac{\partial G}{\partial \tau_{eq}} = 0,$$
$$\frac{\partial G}{\partial \widehat{E}} = 1, \quad \frac{\partial A}{\partial \widehat{E}} = 0, \quad \frac{\partial A}{\partial a_\sigma} = 1.$$

$$\begin{aligned}
\frac{\mathrm{d}T}{\mathrm{d}a_\sigma} &= -\frac{1}{\sqrt{3}} \sum_{\mu=1}^{M} \exp\left(-\frac{\Delta t}{\theta_\mu a_\sigma(t_i)}\right) \frac{\Delta t}{\theta_\mu a_\sigma^2(t_i)} \times \\
&\times \quad \sigma_\mu(t_{i-1}). \\
\frac{\partial G}{\partial a_\sigma} &= \sum_{\mu=1}^{M} \frac{E_\mu}{a_\sigma(t_i)} \exp\left(-\frac{\Delta t}{\theta_\mu a_\sigma(t_i)}\right) - \\
&- \quad \frac{E_\mu \theta_\mu}{\Delta t}\left(1 - \exp\left(-\frac{\Delta t}{\theta_\mu a_\sigma(t_i)}\right)\right). \\
\frac{\partial A}{\partial \tau_{eq}} &= \frac{\cosh\left(\frac{\tau_{eq}(t_i)}{\tau_0}\right) \frac{\tau_{eq}(t_i)}{\tau_0^2} - \frac{1}{\tau_0}\sinh\frac{\tau_{eq}(t_i)}{\tau_0}}{\sinh^2\left(\frac{\tau_{eq}(t_i)}{\tau_0}\right)},
\end{aligned}$$

Since the Newton-Raphson is only locally convergent, the crucial point in a successful implementation is an estimate of the initial solution. This is also the reason, while for very large steps > 60 s the method started to diverge very rapidly. On the contrary, for a "reasonable" time step a forward Euler estimate of the initial solution proved to be a good choice. For the one-dimensional setting the initial conditions are

$$\{\mathsf{a}\} = \begin{Bmatrix} \sigma(t_i) \\ \widehat{E}(\sigma(t_i)) \\ a_\sigma(\sigma(t_i)) \end{Bmatrix}$$
$$\{\mathsf{r}\} = \begin{Bmatrix} \tau_{eq}(t_i) - \widehat{\tau}_{eq}(t_i) \\ 0 \\ 0 \end{Bmatrix}$$

where $\sigma(t_i) = \sigma(t_{i-1}) + \widehat{E}(t_{i-1})\,(\Delta\varepsilon - \widehat{\varepsilon}(t_{i-1}))$ and $\widehat{\tau}_{eq}(t_i) = \frac{1}{\sqrt{3}}\left(\sigma(t_i) + \widehat{E}(t_i)\,(\Delta\varepsilon - \Delta\widehat{\varepsilon}(t_i))\right)$.
The results displayed in Figs. 11- 12 provide further notion about both methods when applied to the present problem. While for the forward (fully) explicit method the results in Fig. 11 show an oscillatory response attributed to the assumed constant stress shift parameter a_σ over a given time step, no such behavior was observed for the backward (fully) implicit method for all time increments marked with the success in convergence of the Newton-Raphson iteration. Finally, Table 8 shows the rate of convergence in terms of the average and maximum number of iterations needed to achieve the given prescribed error.

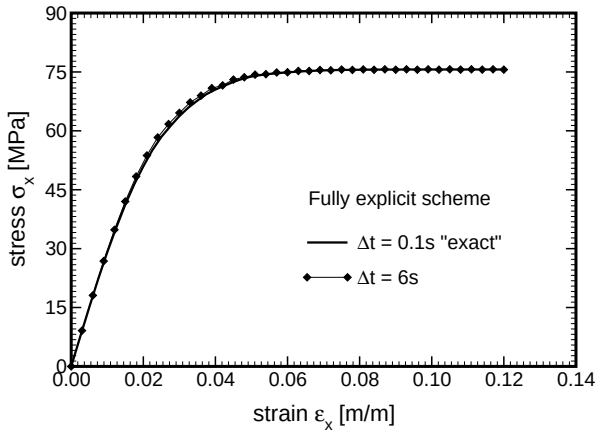

(a)

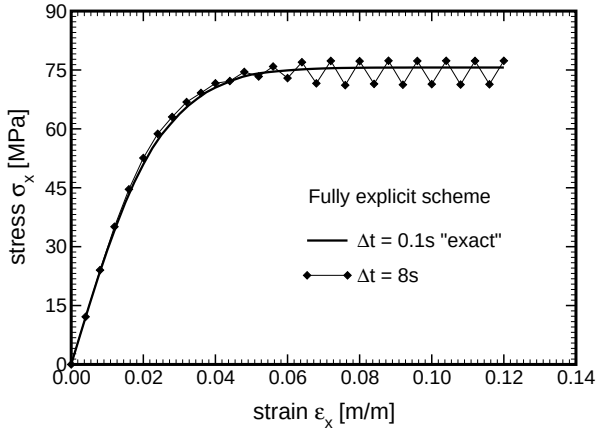

(b)

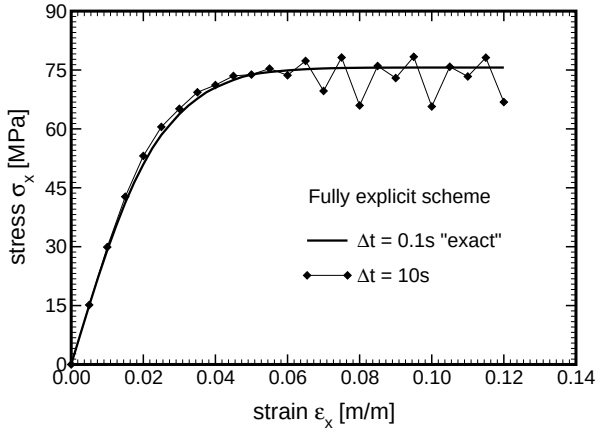

(c)

Figure 11: Fully explicit integration scheme

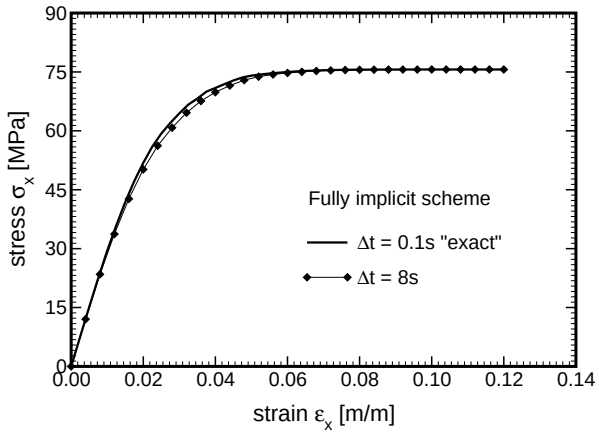

(a)

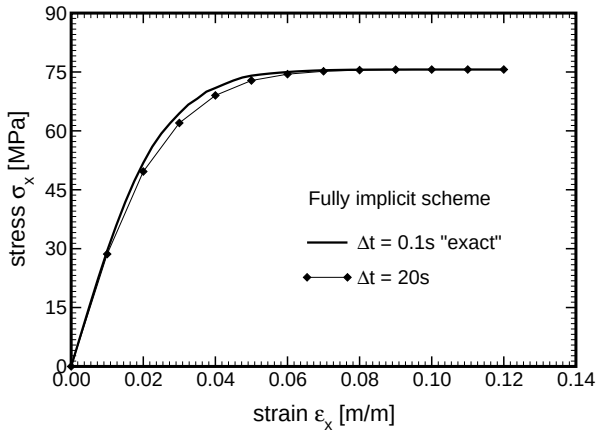

(b)

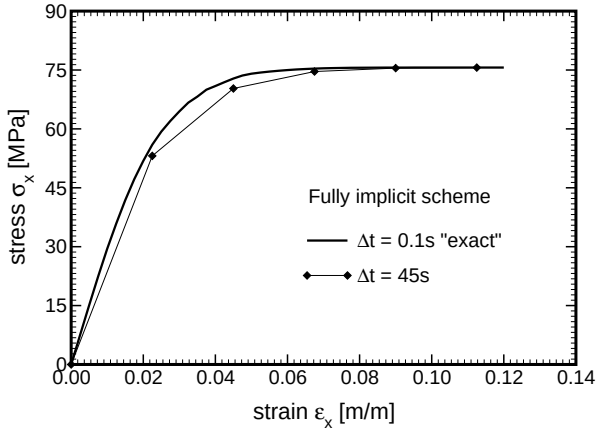

(c)

Figure 12: Fully implicit integration scheme

Time step	Avg. No. of iter.	Max. No. of iter.
8	4	6
20	5	8
30	10	25
40	14	26
45	12	24

Table 8: Number of iterations required to reach a residuum norm $\|\mathsf{r}\| = \sqrt{\{\mathsf{r}\}^{\mathsf{T}}\{\mathsf{r}\}} < 10^{-8}$

References

[Ber68] M. J. Beran. *Statistical Continuum Theories*. Monographs in Statistical Physics. Interscience Publishers, 1968.

[Ber84] J. G. Berryman. Measurement of spatial correlation functions using image processing techniques. *Journal of Applied Physics*, 57(7):2374–2384, 1984.

[BP85] C.S. Burrus and T. W. Parks. *DFT/FFT and convolution algorithms: Theory and implementation*. Topics in Digital Signal Processing. A Wiley-Interscience Publication, 1985.

[BS96] Z. Bittnar and J. Sejnoha. *Numerical methods in structural engineering*. ASCE Press, 1996.

[BS02] J. G. J. Beijer and J. L. Spoormaker. Solution strategies for fem analysis with nonlinear viscoelastic polymers. *Computers & Structures*, 80:1213–1229, 2002.

[CKMP01] J.L. Chaboche, S. Kruch, J.F. Maire, and T. Pottier. Towards a micromechanics based inelastic and damage modeling of composites. *International Journal of Plasticity*, 17(4):411–439, 2001.

[DB92] G. J. Dvorak and Y. Benveniste. On transformation strains and uniform fields in multiphase elastic media. *Proceedings of the Royal Society of London Series A - Mathematical, Physical and Engineering Sciences*, 437(1900):291–310, 1992.

[DBED87] G. J. Dvorak and Y. A. Bahei-El-Din. A bimodal plasticity theory of fibrous composite materials. *Acta Mechanica*, 69:219–241, 1987.

[DS99] G. J. Dvorak and M. V. Srinivas. New estimates of overall properties of heterogeneous solids. *Journal of the Mechanics and Physics of Solids*, 47(4):899–920, 1999.

[Dvo92] G. J. Dvorak. Transformation field analysis of inelastic composite materials. *Proceedings of the Royal Society of London Series A - Mathematical, Physical and Engineering Sciences*, 437(1900):311–327, 1992.

[DW96] W.J. Drugan and J.R. Willis. A micromechanics-based nonlocal constitutive equation and estimates of representative volume element size for elastic composites. *Journal of the Mechanics and Physics of Solids*, 44(4):497–524, 1996.

[DYW94] G. J. Dvorak, Bahei-El-Din Y.A., and A.M. Wafa. Implementation of the transformation field analysis for inelastic composite-materials. *Computational Mechanics*, 14(3):201–228, 1994.

[EJ98] M. Erigo and S.G. Johnson. FFTW: An adaptive software architecture for the FFT. In *Proceedings of the 1998 IEEE International Conference on Acoustics, Speech and Signal Processing, ICASSP98*, volume 3, pages 1381–1384. IEEE, New York, 1998. (See also `http://www.fftw.org`).

[FS00] J. Fish and K. Shek. Multiscale analysis of large-scale nonlinear structures and materials. *International Journal for Computational Civil and Structural Engineering*, 1(1):79–90, 2000.

[FYS99] J. Fish, Q. Yu, and K. Shek. Computational damage mechanics for composite materials based on mathematical homogenization. *International Journal for Numerical Methods in Engineering*, 45(11):1657–1679, 1999.

[HAM04] R. M. Haj-Ali and A. H. Muliana. Numerical finite element formulation of the Schapery non-linear viscoelastic material model. *International Journal for Numerical Methods in Engineering*, 59(1):25–45, 2004.

[HS62] Z. Hashin and S. Shtrikman. On some variational principles in anisotropic and nonhomogeneous elasticity. *Journal of the Mechanics and Physics of Solids*, 10:335–342, 1962.

[HS63] Z. Hashin and S. Shtrikman. A variational approach to the theory of elastic behavior of multiphase materials. *Journal of the Mechanics and Physics of Solids*, 11:127–140, 1963.

[KBB01] V. Kouznetsova, W. A. M. Brekelmans, and P. T. Baaijens. An approach to micro-macro modeling of heterogeneous materials. *Computational Mechanics*, 27(1):37–48, 2001.

[KGB02] V. Kouznetsova, M. G. D. Geers, and W. A. M. Brekelmans. Multi-scale constitutive modelling of heterogeneous materials with a gradient-enhanced computational homogenization scheme. *International Journal for Numerical Methods in Engineering*, 54(8):1235–1260, 2002.

[KL97] R.S. Kody and A. J. Lesser. Deformation and yield of epoxy networks in constrained states of stress. *Journal of Materials Science*, 32(21):5637–5643, 1997.

[Krö86] E. Kröner. Statistical modelling. In J. Gittus and J. Zarka, editors, *Modelling of small deformation of polycrystals*, pages 229–291. Elsevier Applied Science Publishers, 1986.

[Leo76] A. I. Leonov. Non-equilibrium thermodynamics and rheology of viscoelastic polymer media. *Rheol. Acta*, 15:85–98, 1976.

[LGN91] D. C. Lagoudas, A. C. Gavazzi, and H. Nigam. Elastoplastic behavior of metal matrix composites based on incremental plasticity and the Mori-Tanaka averaging scheme. *Computational Mechanics*, 8:193–203, 1991.

[Mar98] K. Z. Markov. On the cluster bounds for the effective properties of microcraked solids. *Journal of the Mechanics and Physics of Solids*, 46(2):357–388, 1998.

[Mas03] T.J. Massart. *Multi-scale modeling of damage in masonry structures*. PhD thesis, Technische Universiteit Eindhoven, 2003.

[Mat03] K. Matouš. Damage evolution in particulate composite materials. *International Journal of Solids and Structures*, 40(6):1489–1503, 2003.

[Mil02] G. W. Milton. *The Theory of Composites*, volume 6 of *Cambridge Monographs on Applied and Computational Mathematics*. Cambridge University Press, 2002.

[MMS99] J. C. Michel, H. Moulinec, and P. Suquet. Effective properties of composite materials with periodic microstructure: A computational approach. *Computer Methods in Applied Mechanics and Engineering*, 172:109–143, 1999.

[Mur87] T. Mura. *Micromechanics of Defects in Solids*. Number 3 in Mechanics of elastic and inelastic solids. Kluwer Academic Publishers, second revised edition, 1987.

[Pov95] G. L. Povirk. Incorporation of microstructural information into models of two-phase materials. *Acta metallurgica et materialia*, 43(8):3199–3206, 1995.

[PS03] P. Procházka and J. Sejnoha. A BEM formulation for homogenization of composites with randomly distributed fibers. *Engineering Analysis with Boundary Elements*, 27(2):137–144, 2003.

[Sch69] R. A. Schapery. Further development of thermodynamic constitutive theory: Stress formulation. Technical report, Purdue Res. Foundation, Project No. 4958, February 1969.

[SG02] Z. Shan and A.M. Gokhale. Representative volume element for non-uniform microstructures. *Computational Materials Science*, 24:361–379, 2002.

[SM99] M. Sejnoha and K. Matouš. Nonlinear analysis of intially prestressed laminates. In Z. Bittnar, editor, *Contributions to Computational Mechanics in Civil Engineering*, volume 3 of *CTU Reports*, pages 55–68. CTU in Prague, 1999.

[SZ02a] M. Sejnoha and J. Zeman. *Micromechanical analysis of random composites*, volume 6 of *CTU Reports*. Czech Technical University in Prague, 2002.

[SZ02b] M. Sejnoha and J. Zeman. Overall viscoelastic response of random fibrous composites with statistically quasi uniform distribution of reinforcements. *Computer Methods in Applied Mechanics and Engineering*, 191(44):5027–5044, 2002.

[SZS00] M. Sejnoha, J. Zeman, and J. Sejnoha. Evaluation of effective thermoelastic properties of random fibrous composites. *International Journal for Engineering Modelling*, 13(3–4):61–68, 2000.

[TD88] J. L. Teplý and G. J. Dvorak. Bound on overall instantaneous properties of elastic-plastic composites. *Journal of the Mechanics and Physics of Solids*, 36(1):29–58, 1988.

[Ter96] T. A. Tervoort. *Constitutive modeling of polymer glasses: Finite, nonlinear visocelastic behaviour of polycarbonate*. PhD thesis, Eindhoven University of Technology, Eindhoven, 1996.

[Tor02] S. Torquato. *Random heterogeneous materials: Microstructure and macroscopic properties*. Springer-Verlag, 2002.

[TS82] S. Torquato and G. Stell. Microstructure of two-phase random media.I. The n-point probability functions. *Journal of Chemical Physics*, 77(4):2071–2077, 1982.

[VS03] R. Valenta and M. Sejnoha. Simulation of time dependent behaviour of epoxy matrices – From experiment to numerical analysis. In preparation, 2003.

[Wie00] M. Wierer. Homogenization of woven composites on meso-scale. In Z. Bittnar and J. Sejnoha, editors, *Contributions to mechanics of materials and structures*, volume 4 of *CTU Reports*, pages 195–204. CTU in Prague, 2000.

[Wil77] J. R. Willis. Bounds and self-consistent estimates for the overall properties of anisotropic composites. *Journal of the Mechanics and Physics of Solids*, 25:185–202, 1977.

[Wil81] J. R. Willis. Variational and related methods for the overall properties of composites. In *Advances in Applied Mechanics*, volume 21, pages 2–74, 1981.

[Zem03] J. Zeman. *Analysis of composite materials with random microstructure*, volume 7 of *CTU Reports*. CTU in Prague, 2003. 177 pp.

[ZS01] J. Zeman and M. Sejnoha. Numerical evaluation of effective properties of graphite fiber tow impregnated by polymer matrix. *Journal of the Mechanics and Physics of Solids*, 49(1):69–90, 2001.

[ZS03] J. Zeman and M. Sejnoha. Homogenization of balanced plain weave composites with imperfect microstructure: Part i – theoretical formulation. *International Journal for Solids and Structures*, 2003. Submitted for publication.